

1 Quasi-consistent efficient meshfree thin shell
2 formulation with penalty-free essential boundary
3 condition enforcement

4 Junchao Wu^{a,*}, Yangtao Xu^a, Bin Xu^a, Syed Humayun Basha^a

^a*Key Laboratory for Intelligent Infrastructure and Monitoring of Fujian Province, Key Laboratory for Structural Engineering and Disaster Prevention of Fujian Province, College of Civil Engineering, Huaqiao University, Xiamen, Fujian, 361021, China*

5 **Abstract**

This research proposed an efficient and quasi-consistent meshfree thin shell formulation with penalty-free enforcement of essential boundary conditions. Within the framework of the Hu-Washizu variational principle, a mixed formulation of displacements, strains and stresses is employed in this approach, where the displacements are discretized using meshfree shape functions, and the strains and stresses are expressed using smoothed gradients, covariant smoothed gradients and covariant bases. The smoothed gradients satisfy the first second-order integration constraint and have variational consistency for polynomial strains and stresses. Owing to Hu-Washizu variational principle, the essential boundary conditions automatically arise in its weak form. As a result, the suggested technique's enforcement of essential boundary conditions resembles that of the traditional Nitsche's method. Contrary to Nitsche's method, the costly higher order derivatives of conventional meshfree shape functions were replaced by the smoothed gradients with fast computation, which improve the efficiency. Meanwhile, the proposed formulation features a naturally stabilized term without adding any artificial stabilization factors, which eliminates the employment of penalty method as a stabilization. The efficacy of the proposed Hu-Washizu meshfree thin shell formulation is illustrated by a set of classical standard thin shell problems.

6 *Keywords:* Meshfree, Thin shell, Hu-Washizu variational principle,
7 Reproducing kernel gradient smoothing, Essential boundary condition

*Corresponding author
Email address: jcwu@hqu.edu.cn (Junchao Wu)

8 **1. Introduction**

9 Thin shell structures generally adhere to the Kirchhoff hypothesis [1], that
10 neglects the shear deformation can be described using Galerkin formulation
11 which requires to have at least C^1 continuity. The traditional finite element
12 methods usually only have C^0 continuous shape functions, and it prefers Mindlin
13 thick shear theory, hybrid and mixed models in simulation of shell structure [2].
14 Meshfree methods [3, 4, 5] with high order smoothed shape functions have gar-
15 nered much research attention over the past thirty years. These techniques
16 established the shape functions based on a collection of dispersed nodes, and
17 the high order continuity of shape functions can be easily achieved even with
18 low-order basis functions. For thin shell analysis, this high order meshfree ap-
19 proximation can also alleviate the membrane locking caused by the mismatched
20 approximation order of membrane strain and bending strain [6]. Furthermore,
21 nodal-based meshfree approximations generally offer the flexibility of local re-
22 finement and can relieve the burden of mesh distortion. Owing to these benefits,
23 numerous meshfree techniques have been developed and implemented in many
24 scientific and engineering fields [7, 8, 9, 10, 11, 12, 13]. However, the high order
25 smoothed meshfree shape functions accompany the enlarged and overlapping
26 supports, which may potentially cause many problems for shape functions. One
27 of the issues is the loss of the Kronecker delta property, which means that, un-
28 like the finite element methods, the necessary boundary conditions cannot be
29 directly enforced [14]. Another issue is that the variational consistency or said
30 integration constraint, which is a condition requires the formulation to exactly
31 reproduce the solution spanned by basis functions, cannot be satisfied. This
32 issue is caused by the misalignment between the numerical integration domains
33 and supports of shape functions, and thus, the shape functions exhibit to a
34 piecewise nature in each integration domain. It turns to that the traditional
35 integration rules like Gauss scheme cannot ensure the integration accuracy in
36 Galerkin weak form [15, 16]. Therefore, variational consistency is vital to the
37 solution accuracy in Galerkin formulations.

38 Various ways have been presented to enforce the necessary boundary for
39 Galerkin meshfree methods directly, including the boundary singular kernel
40 method [17], mixed transformation method [17], and interpolation element-free
41 method [18] for recovering shape functions' Kronecker property. However, these
42 methods are not based on a variational setting and cannot guarantee varia-
43 tional consistency. In the absence of a meshfree node, accuracy enforcement
44 might be poorer. In contrast, enforcing the essential boundary conditions using
45 a variational approach is preferred for Galerkin meshfree methods. The varia-
46 tional consistent Lagrange multiplier approach was initially used to the Galerkin
47 meshfree method by Belytschko et al. [3]. In this method, the extra degrees
48 of freedom are used to determine the discretion of Lagrange multiplier. Fur-
49 thermore, Ivannikov et al. [19] have extended this approach to geometrically
50 nonlinear thin shells. Lu et al. [20] suggested the modified variational es-
51 sential boundary enforcement approach and expressed the Lagrange multiplier
52 by equivalent tractions to eliminate the excess degrees of freedom. However,

53 the coercivity of this approach is not always ensured and potentially reduces
54 the accuracy. Zhu and Atluri [21] pioneered the penalty method for meshfree
55 method, making it a straightforward approach to enforce essential boundary
56 conditions via Galerkin weak form. However, the penalty method lacks varia-
57 tional consistency and requires experimental artificial parameters whose optimal
58 value is hard to determine. Fernández-Méndez and Huerta [14] imposed neces-
59 sary boundary conditions using Nitsche’s approach in the meshfree formulation.
60 This approach can be seen as a hybrid combination of the modified variational
61 method and the penalty method because the modified variational method gen-
62 erates variational consistency through the use of a consistent term, and the
63 penalty method is used as a stabilized term to recover the coercivity. Skatulla
64 and Sansour [22] extended Nitsche’s thin shell analysis method and proposed an
65 iteration algorithm to determine artificial parameters at each integration point.

66 In order to address the issue of numerical integration, a series of consis-
67 tent integration schemes have been developed for Galerkin meshfree methods.
68 Among these include stabilized conforming nodal integration [23], variational
69 consistent integration [24], quadratic consistent integration [25], reproducing
70 kernel gradient smoothing integration [26], and consistent projection integration
71 [27]. The assumed strain approach establishes the most consistent integration
72 scheme, while the smoothed gradient replaces the costly higher order derivatives
73 of traditional meshfree shape functions and shows a high efficiency. Moreover,
74 to achieve global variational consistency, a consistent essential boundary con-
75 dition enforcement should cooperate with the consistent integration scheme.
76 The consistent integration scheme and Nitsche’s method for treating essential
77 boundary conditions show a good performance since they can satisfy the coer-
78 civity without requiring additional degrees of freedom. Nevertheless, Nitsche’s
79 approach still retains the artificial parameters in stabilized terms, and it is es-
80 sential to remain conscious of the costly higher order derivatives, particularly
81 for thin plate and thin shell problems. Recently, Wu et al. [28, 29] proposed
82 an efficient and stabilized essential boundary condition enforcement method
83 based upon the Hellinger-Reissner variational principle, where a mixed formu-
84 lation in Hellinger-Reissner weak form recasts the reproducing kernel gradient
85 smoothing integration. The terms for enforcing essential boundary conditions
86 are identical to the Nitsche’s method, and both have consistent and stabilized
87 terms. Nevertheless, the stabilized term of this method naturally exists in the
88 Hellinger-Reissner weak form and no longer needs the artificial parameters, even
89 for essential boundary enforcement; instead all of the higher order derivatives
90 are represented by smoothed gradients and their derivatives.

91 In this study, an efficient and stabilized variational consistent meshfree
92 method that naturally enforces the essential boundary conditions is developed
93 for thin shell structure. Following the concept of the Hellinger-Reissner prin-
94 ciple base consistent meshfree method, the Hu-Washizu variational principle of
95 complementary energy with variables of displacement, strains, and stresses is
96 employed. The displacement is approximated by conventional meshfree shape
97 functions, and the strains and stresses are expressed by smoothed gradients with
98 covariant bases. It is important to note that although the first second-order in-

99 tegration requirements are naturally embedded in the smoothed gradients, their
100 fulfillment can only result in a quasi-satisfaction of variational consistency be-
101 cause of the non-polynomial nature of the stresses. Hu-Washizu's weak form is
102 used to evaluate all the essential boundary conditions regarding displacements
103 and rotations. This type of formulation is similar to the Nitsche's method but
104 does not require any artificial parameters. Compared with Nitsche's method,
105 conventional reproducing smoothed gradients and its direct derivatives replace
106 the costly higher order derivatives. By utilizing the advantages of a replicating
107 kernel gradient smoothing framework, the smoothed gradients showed better
108 performance compared to conventional derivatives of shape functions, hence
109 increasing the meshfree formulation's computational efficiency.

110 The remainder of this research paper is structured as follows: The kinematics
111 of the thin shell structure and the weak form of the associated Hu-Washizu
112 principle are briefly described in Section 2. Subsequently, the mixed formulation
113 regarding the displacements, strains and stresses in accordance with Hu-Washizu
114 weak form are presented in Section 3. The discrete equilibrium equations are
115 derived in Section 4 using the naturally occurring accommodation of essential,
116 and they are compared to the equations obtained using Nitsche's method. The
117 numerical results in Section 5 validate the efficacy of the proposed Hu-Washizu
118 meshfree thin shell formulation. Lastly, the concluding remarks are presented
119 in Section 6.

120 **2. Hu-Washizu's formulation of complementary energy for thin shell**

121 *2.1. Kinematics for thin shell*

122 Consider the configuration of a shell $\bar{\Omega}$, as shown in Fig. 1, which can be
 123 easily described by a parametric curvilinear coordinate system $\xi = \{\xi^i\}_{i=1,2,3}$.
 124 The mid-surface of the shell denoted by Ω is specified by the in-plane coordinates
 125 $\xi = \{\xi^\alpha\}_{\alpha=1,2}$, as the thickness direction of shell is by ξ^3 , $-\frac{h}{2} \leq \xi^3 \leq \frac{h}{2}$, h is
 126 the thickness of shell. In this work, Latin indices take the values from 1 to 3,
 127 and Greek indices are evaluated by 1 or 2. For the Kirchhoff hypothesis [6], the
 128 position $\mathbf{x} \in \bar{\Omega}$ is defined by linear functions with respect to ξ^3 :

$$\mathbf{x}(\xi^1, \xi^2, \xi^3) = \mathbf{r}(\xi^1, \xi^2) + \xi^3 \mathbf{a}_3(\xi^1, \xi^2) \quad (1)$$

in which \mathbf{r} means the position on the mid-surface of shell, and \mathbf{a}_3 is correspond-

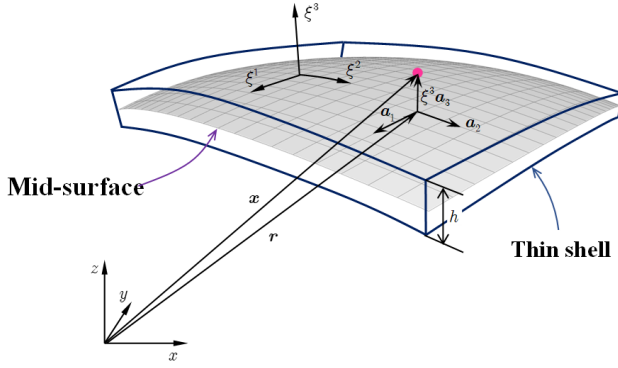


Figure 1: Kinematics for thin shell.

129
 130 ing normal direction. For the mid-surface of shell, the in-plane covariant base
 131 vector with respect to ξ^α can be derived by a trivial partial differentiation to \mathbf{r} :

$$\mathbf{a}_\alpha = \frac{\partial \mathbf{r}}{\partial \xi^\alpha} = \mathbf{r}_{,\alpha}, \alpha = 1, 2 \quad (2)$$

132 to provide for a clear expression, the subscript comma denotes the partial dif-
 133 ferentiation operation with respect to in-plane coordinates ξ^α , and the normal
 134 vector \mathbf{a}_3 can be obtained by the normalized cross product of \mathbf{a}_α 's as follows:

$$\mathbf{a}_3 = \frac{\mathbf{a}_1 \times \mathbf{a}_2}{\|\mathbf{a}_1 \times \mathbf{a}_2\|} \quad (3)$$

135 where $\|\bullet\|$ is the Euclidean norm operator.

136 With the assumption of infinitesimal deformation, the strain components
 137 with respect to the global contravariant base can be stated as:

$$\epsilon_{ij} = \frac{1}{2} (\mathbf{x}_{,i} \cdot \mathbf{u}_{,j} + \mathbf{u}_{,i} \cdot \mathbf{x}_{,j}) \quad (4)$$

¹³⁸ where \mathbf{u} represents the displacement for the shell deformation. To satisfy the
¹³⁹ Kirchhoff hypothesis, the displacement is assumed to be of the following form:

$$\mathbf{u}(\xi^1, \xi^2, \xi^3) = \mathbf{v}(\xi^1, \xi^2) + \boldsymbol{\theta}(\xi^1, \xi^2)\xi^3 \quad (5)$$

¹⁴⁰ in which the quadratic and higher order terms are neglected. $\mathbf{v}, \boldsymbol{\theta}$ represent
¹⁴¹ the displacement and rotation in mid-surface, respectively.

¹⁴² Subsequently, plugging Eqs. (1) and (5) into Eq. (4) and neglecting the
¹⁴³ quadratic terms, the strain components can be rephrased as follows:

$$\begin{aligned} \epsilon_{\alpha\beta} &= \frac{1}{2}(\mathbf{a}_\alpha \cdot \mathbf{v}_{,\beta} + \mathbf{v}_{,\alpha} \cdot \mathbf{a}_\beta) \\ &\quad + \frac{1}{2}(\mathbf{a}_{3,\alpha} \cdot \mathbf{v}_{,\beta} + \mathbf{v}_{,\alpha} \cdot \mathbf{a}_{3,\beta} + \mathbf{a}_\alpha \cdot \boldsymbol{\theta}_{,\beta} + \boldsymbol{\theta}_{,\alpha} \cdot \mathbf{a}_\beta)\xi^3 \end{aligned} \quad (6a)$$

$$\epsilon_{\alpha\beta} = \varepsilon_{\alpha\beta} + \kappa_{\alpha\beta}\xi^3 \quad (6b)$$

$$\epsilon_{33} = \mathbf{a}_3 \cdot \boldsymbol{\theta} \quad (6c)$$

¹⁴⁴ where $\varepsilon_{\alpha\beta}, \kappa_{\alpha\beta}$ represent membrane and bending strains, respectively, and are
¹⁴⁵ given as follows:

$$\varepsilon_{\alpha\beta} = \frac{1}{2}(\mathbf{a}_\alpha \cdot \mathbf{v}_{,\beta} + \mathbf{v}_{,\alpha} \cdot \mathbf{a}_\beta) \quad (7)$$

$$\kappa_{\alpha\beta} = \frac{1}{2}(\mathbf{a}_{3,\alpha} \cdot \mathbf{v}_{,\beta} + \mathbf{v}_{,\alpha} \cdot \mathbf{a}_{3,\beta} + \mathbf{a}_\alpha \cdot \boldsymbol{\theta}_{,\beta} + \boldsymbol{\theta}_{,\alpha} \cdot \mathbf{a}_\beta) \quad (8)$$

¹⁴⁷ In accordance with the Kirchhoff hypothesis, the thickness of shell will not
¹⁴⁸ change, and the deformation related with direction of ξ^3 will vanish, i.e. $\epsilon_{3i} = 0$.
¹⁴⁹ Thus, the rotation $\boldsymbol{\theta}$ can be rewritten as:

$$\epsilon_{3i} = 0 \Rightarrow \begin{cases} \boldsymbol{\theta} \cdot \mathbf{a}_\alpha = -\mathbf{v}_{,\alpha} \cdot \mathbf{a}_3 \\ \boldsymbol{\theta} \cdot \mathbf{a}_3 = 0 \end{cases} \Rightarrow \boldsymbol{\theta} = -\mathbf{v}_{,\alpha} \cdot \mathbf{a}_3 \mathbf{a}^\alpha \quad (9)$$

¹⁵⁰ where \mathbf{a}^α 's is the in-plane contravariant base vector, $\mathbf{a}^\alpha \cdot \mathbf{a}_\beta = \delta_\beta^\alpha$, δ is the
¹⁵¹ Kronecker delta function. The detailed derivation of Eq. 9 can be found in
¹⁵² reference [30].

¹⁵³ Furthermore, substituting Eq. (9) into Eq. (8) leads to:

$$\kappa_{\alpha\beta} = (\Gamma_{\alpha\beta}^\gamma \mathbf{v}_{,\gamma} - \mathbf{v}_{,\alpha\beta}) \cdot \mathbf{a}_3 = -\mathbf{v}_{,\alpha\beta} \cdot \mathbf{a}_3 \quad (10)$$

¹⁵⁴ in which $\Gamma_{\alpha\beta}^\gamma = \mathbf{a}_{\alpha,\beta} \cdot \mathbf{a}^\gamma$ is namely the Christoffel symbol of the second kind,
¹⁵⁵ and $\mathbf{v}_{,\alpha\beta}$ is the in-plane covariant derivative of $\mathbf{v}_{,\alpha}$, i.e. $\mathbf{v}_{,\alpha\beta} = \Gamma_{\alpha\beta}^\gamma \mathbf{v}_{,\gamma} - \mathbf{v}_{,\alpha\beta}$.

¹⁵⁶ 2.2. Galerkin weak form for Hu-Washizu principle of complementary energy

¹⁵⁷ In this study, the Hu-Washizu variational principle of complementary energy
¹⁵⁸ [31] was adopted for the development of the proposed analytical approach, the

¹⁵⁹ corresponding complementary functional, denoted by Π_C , is listed as follows:

$$\begin{aligned} & \Pi_C(\varepsilon_{\alpha\beta}, \kappa_{\alpha\beta}, N^{\alpha\beta}, M^{\alpha\beta}) \\ &= \int_{\Omega} \frac{h}{2} \varepsilon_{\alpha\beta} C^{\alpha\beta\gamma\eta} \varepsilon_{\gamma\eta} d\Omega + \int_{\Omega} \frac{h^3}{24} \kappa_{\alpha\beta} C^{\alpha\beta\gamma\eta} \kappa_{\gamma\eta} d\Omega \\ &+ \int_{\Omega} \varepsilon_{\alpha\beta} (N^{\alpha\beta} - h C^{\alpha\beta\gamma\eta} \varepsilon_{\gamma\eta}) d\Omega + \int_{\Omega} \kappa_{\alpha\beta} (M^{\alpha\beta} - \frac{h^3}{12} C^{\alpha\beta\gamma\eta} \kappa_{\gamma\eta}) d\Omega \\ &- \int_{\Gamma_v} \mathbf{T} \cdot \bar{\mathbf{v}} d\Gamma + \int_{\Gamma_\theta} M_{\mathbf{n}\mathbf{n}} \bar{\theta}_{\mathbf{n}} d\Gamma - (P \mathbf{a}_3 \cdot \bar{\mathbf{v}})_{\mathbf{x} \in C_w} \end{aligned} \quad (11)$$

¹⁶⁰ where $C^{\alpha\beta\gamma\eta}$'s represent the components of fourth order elasticity tensor with
¹⁶¹ respect to the covariant base and plane stress assumption, and it can be ex-
¹⁶² pressed by Young's modulus E , Poisson's ratio ν and the in-plane contravariant
¹⁶³ metric coefficients $a^{\alpha\beta}$'s, $a^{\alpha\beta} = \mathbf{a}^\alpha \cdot \mathbf{a}^\beta$, as follows:

$$C^{\alpha\beta\gamma\eta} = \frac{E}{2(1+\nu)} (a^{\alpha\gamma} a^{\beta\eta} + a^{\alpha\eta} a^{\beta\gamma} + \frac{2\nu}{1-\nu} a^{\alpha\beta} a^{\gamma\eta}) \quad (12)$$

¹⁶⁴ and $N^{\alpha\beta}$, $M^{\alpha\beta}$ are the components of membrane and bending stresses given by:

$$N^{\alpha\beta} = h C^{\alpha\beta\gamma\eta} \varepsilon_{\gamma\eta}, \quad M^{\alpha\beta} = \frac{h^3}{12} C^{\alpha\beta\gamma\eta} \kappa_{\gamma\eta} \quad (13)$$

¹⁶⁵ Essential boundaries on the edges and corners denoted by Γ_v , Γ_θ and C_v are
¹⁶⁶ naturally existed in complementary energy functional, $\bar{\mathbf{v}}$, $\bar{\theta}_{\mathbf{n}}$ are the correspond-
¹⁶⁷ ing prescribed displacement and normal rotation, respectively. \mathbf{T} , $M_{\mathbf{n}\mathbf{n}}$ and P
¹⁶⁸ can be determined by Euler-Lagrange equations of shell problem [30] as follows:

$$\mathbf{T} = \mathbf{T}_N + \mathbf{T}_M \rightarrow \begin{cases} \mathbf{T}_N = \mathbf{a}_\alpha N^{\alpha\beta} n_\beta \\ \mathbf{T}_M = (\mathbf{a}_3 M^{\alpha\beta} s_\alpha n_\beta)_{,\gamma} s^\gamma + (\mathbf{a}_3 M^{\alpha\beta})|_\beta n_\alpha \end{cases} \quad (14)$$

$$M_{\mathbf{n}\mathbf{n}} = M^{\alpha\beta} n_\alpha n_\beta \quad (15)$$

$$P = -[[M^{\alpha\beta} s_\alpha n_\beta]] \quad (16)$$

¹⁷¹ where $\mathbf{n} = n^\alpha \mathbf{a}_\alpha = n_\alpha \mathbf{a}^\alpha$ and $\mathbf{s} = s^\alpha \mathbf{a}_\alpha = s_\alpha \mathbf{a}^\alpha$ are the outward normal and
¹⁷² tangent directions on boundaries. $[[f]]$ is the jump operator defined by:

$$[[f]]_{\mathbf{x}=\mathbf{x}_c} = \lim_{\epsilon \rightarrow 0^+} (f(\mathbf{x}_c + \epsilon) - f(\mathbf{x}_c - \epsilon)), \mathbf{x}_c \in \Gamma \quad (17)$$

¹⁷³ where f is an arbitrary function on Γ .

¹⁷⁴ Moreover, the natural boundary conditions should be applied by Lagrangian
¹⁷⁵ multiplier method with displacement \mathbf{v} regarded as multiplier. Thus, then the
¹⁷⁶ new complementary energy functional namely Π is given by:

$$\begin{aligned} & \Pi(\mathbf{v}, \varepsilon_{\alpha\beta}, \kappa_{\alpha\beta}, N^{\alpha\beta}, M^{\alpha\beta}) \\ &= \Pi_C(\varepsilon_{\alpha\beta}, \kappa_{\alpha\beta}, N^{\alpha\beta}, M^{\alpha\beta}) + \int_{\Gamma_M} \theta_{\mathbf{n}} (M_{\mathbf{n}\mathbf{n}} - \bar{M}_{\mathbf{n}\mathbf{n}}) d\Gamma \\ &- \int_{\Gamma_T} \mathbf{v} \cdot (\mathbf{T} - \bar{\mathbf{T}}) d\Gamma - \mathbf{v} \cdot \mathbf{a}_3 (P - \bar{P})_{\mathbf{x} \in C_P} - \int_{\Omega} \mathbf{v} \cdot (\mathbf{b} - \bar{\mathbf{b}}) d\Omega \end{aligned} \quad (18)$$

¹⁷⁷ where $\bar{\mathbf{T}}$, \bar{M}_{nn} and \bar{P} are the prescribed traction, bending moment and concentrated force on edges Γ_T , Γ_M and corner C_P respectively. All the boundaries ¹⁷⁸ meet the following geometric relationships:

$$\begin{cases} \Gamma = \Gamma_v \cup \Gamma_T \cup \Gamma_\theta \cup \Gamma_M, & C = C_v \cup C_P, \\ \Gamma_v \cap \Gamma_T = \Gamma_\theta \cap \Gamma_M = C_v \cap C_P = \emptyset \end{cases} \quad (19)$$

¹⁸⁰ and $\bar{\mathbf{b}}$ stands for the prescribed body force in Ω , \mathbf{b} also can be written based on ¹⁸¹ Euler-Lagrange equations [30] as:

$$\mathbf{b} = \mathbf{b}_N + \mathbf{b}_M \rightarrow \begin{cases} \mathbf{b}_N = (\mathbf{a}_\alpha N^{\alpha\beta})|_\beta \\ \mathbf{b}_M = (\mathbf{a}_3 M^{\alpha\beta})|_{\alpha\beta} \end{cases} \quad (20)$$

¹⁸² Introducing a standard variational argument to Eq. (18), $\delta\Pi = 0$, and ¹⁸³ considering the arbitrariness of virtual variables, $\delta\mathbf{v}$, $\delta\varepsilon_{\alpha\beta}$, $\delta\kappa_{\alpha\beta}$, $N^{\alpha\beta}$, $M^{\alpha\beta}$ ¹⁸⁴ lead to the following weak form:

$$-\int_{\Omega} h\delta\varepsilon_{\alpha\beta}C^{\alpha\beta\gamma\eta}\varepsilon_{\gamma\eta}d\Omega + \int_{\Omega} \delta\varepsilon_{\alpha\beta}N^{\alpha\beta}d\Omega = 0 \quad (21a)$$

$$-\int_{\Omega} \frac{h^3}{12}\delta\kappa_{\alpha\beta}C^{\alpha\beta\gamma\eta}\kappa_{\gamma\eta}d\Omega + \int_{\Omega} \delta\kappa_{\alpha\beta}M^{\alpha\beta}d\Omega = 0 \quad (21b)$$

$$\begin{aligned} \int_{\Omega} \delta N^{\alpha\beta}\varepsilon_{\alpha\beta}d\Omega - \int_{\Gamma} \delta\mathbf{T}_N \cdot \mathbf{v}d\Gamma + \int_{\Omega} \delta\mathbf{b}_N \cdot \mathbf{v}d\Omega \\ + \int_{\Gamma_v} \delta\mathbf{T}_N \cdot \mathbf{v}d\Gamma = \int_{\Gamma_v} \delta\mathbf{T}_N \cdot \bar{\mathbf{v}}d\Gamma \end{aligned} \quad (21c)$$

$$\begin{aligned} \int_{\Omega} \delta M^{\alpha\beta}\kappa_{\alpha\beta}d\Omega - \int_{\Gamma} \delta M_{nn}\theta_n d\Gamma + \int_{\Gamma} \delta\mathbf{T}_M \cdot \mathbf{v}d\Gamma + (\delta P\mathbf{a}_3 \cdot \mathbf{v})_{\mathbf{x} \in C} + \int_{\Omega} \delta\mathbf{b}_M \cdot \mathbf{v}d\Omega \\ + \int_{\Gamma_\theta} \delta M_{nn}\theta_n d\Gamma - \int_{\Gamma_v} \delta\mathbf{T}_M \cdot \mathbf{v}d\Gamma - (\delta P\mathbf{a}_3 \cdot \mathbf{v})_{\mathbf{x} \in C_v} \\ = \int_{\Gamma_\theta} \delta M_{nn}\bar{\theta}_n d\Gamma - \int_{\Gamma_v} \delta\mathbf{T}_M \cdot \bar{\mathbf{v}}d\Gamma - (\delta P\mathbf{a}_3 \cdot \bar{\mathbf{v}})_{\mathbf{x} \in C_v} \end{aligned} \quad (21d)$$

$$\begin{aligned} \int_{\Gamma} \delta\theta_n M_{nn}d\Gamma - \int_{\Gamma} \delta\mathbf{v} \cdot \mathbf{T}d\Gamma - (\delta\mathbf{v} \cdot \mathbf{a}_3 P)_{\mathbf{x} \in C} + \int_{\Omega} \delta\mathbf{v} \cdot \mathbf{b}d\Omega \\ - \int_{\Gamma_\theta} \delta\theta_n M_{nn}d\Gamma + \int_{\Gamma_v} \delta\mathbf{v} \cdot \mathbf{T}d\Gamma + (\delta\mathbf{v} \cdot \mathbf{a}_3 P)_{\mathbf{x} \in C_v} = - \int_{\Gamma_T} \delta\mathbf{v} \cdot \bar{\mathbf{t}}d\Gamma - \int_{\Omega} \delta\mathbf{v} \cdot \bar{\mathbf{b}}d\Omega \end{aligned} \quad (21e)$$

¹⁸⁹ where the geometric relationships of Eq. (19) is used herein.

190 **3. Mixed meshfree formulation for modified Hellinger-Reissner weak
191 form**

192 *3.1. Reproducing kernel approximation for displacement*

193 This study approximates the displacement by adopting reproducing kernel
194 approximation. As shown in Fig. 2, the mid-surface of the shell Ω is discretized
195 by a set of meshfree nodes $\{\xi_I\}_{I=1}^{n_p}$ in parametric configuration, where n_p is the
196 total number of meshfree nodes. The approximated displacement namely \mathbf{v}^h
197 can be expressed as:

$$\mathbf{v}(\xi) = \sum_{I=1}^{n_p} \Psi_I(\xi) \mathbf{d}_I \quad (22)$$

198 in which Ψ_I and \mathbf{d}_I is the shape function and nodal coefficient tensor related by
199 node ξ_I . According to reproducing kernel approximation [4], the shape function
200 takes the following form:

$$\Psi_I(\xi) = \mathbf{p}^T(\xi) \mathbf{c}(\xi) \phi(\xi_I - \xi) \quad (23)$$

201 where \mathbf{p} is the basis function vector represented using the following quadratic
202 function as:

$$\mathbf{p} = \{1, \xi^1, \xi^2, (\xi^1)^2, \xi^1 \xi^2, (\xi^2)^2\}^T \quad (24)$$

203 The kernel function denoted by ϕ controls the support and smoothness of
204 meshfree shape functions. The quintic B-spline function with square support is
205 used herein as the kernel function:

$$\phi(\xi_I - \xi) = \phi(\hat{s}_1)\phi(\hat{s}_2), \quad \hat{s}_\alpha = \frac{|\xi_I^\alpha - \xi^\alpha|}{s_{\alpha I}} \quad (25)$$

206 with

$$\phi(\hat{s}_\alpha) = \frac{1}{5!} \begin{cases} (3 - 3\hat{s}_\alpha)^5 - 6(2 - 3\hat{s}_\alpha)^5 + 15(1 - 3\hat{s}_\alpha)^5 & \hat{s}_\alpha \leq \frac{1}{3} \\ (3 - 3\hat{s}_\alpha)^5 - 6(2 - 3\hat{s}_\alpha)^5 & \frac{1}{3} < \hat{s}_\alpha \leq \frac{2}{3} \\ (3 - 3\hat{s}_\alpha)^5 & \frac{2}{3} < \hat{s}_\alpha \leq 1 \\ 0 & \hat{s}_\alpha > 1 \end{cases} \quad (26)$$

207 and $s_{\alpha I}$ means the support size of meshfree shape function Ψ_I .

208 The unknown vector \mathbf{c} in shape function are determined by the fulfillment
209 of the so-called consistency condition:

$$\sum_{I=1}^{n_p} \Psi_I(\xi) \mathbf{p}(\xi_I) = \mathbf{p}(\xi) \quad (27)$$

210 or equivalently

$$\sum_{I=1}^{n_p} \Psi_I(\xi) \mathbf{p}(\xi_I - \xi) = \mathbf{p}(\mathbf{0}) \quad (28)$$

²¹¹ Substituting Eq. (22) into (28), yields:

$$\mathbf{A}(\boldsymbol{\xi})\mathbf{c}(\boldsymbol{\xi}) = \mathbf{p}(\mathbf{0}) \Rightarrow \mathbf{c}(\boldsymbol{\xi}) = \mathbf{A}^{-1}(\boldsymbol{\xi})\mathbf{p}(\mathbf{0}) \quad (29)$$

²¹² where \mathbf{A} is the moment matrix:

$$\mathbf{A}(\boldsymbol{\xi}) = \sum_{I=1}^{n_p} \phi(\boldsymbol{\xi}_I - \boldsymbol{\xi}) \mathbf{p}(\boldsymbol{\xi}_I - \boldsymbol{\xi}) \mathbf{p}^T(\boldsymbol{\xi}_I - \boldsymbol{\xi}) \quad (30)$$

²¹³ Substituting Eq. (29) back into Eq. (22), the expression of meshfree shape
²¹⁴ function can be written as:

$$\Psi_I(\boldsymbol{\xi}) = \mathbf{p}^T(\boldsymbol{\xi}_I - \boldsymbol{\xi}) \mathbf{A}^{-1}(\boldsymbol{\xi}) \mathbf{p}(\mathbf{0}) \phi(\boldsymbol{\xi}_I - \boldsymbol{\xi}) \quad (31)$$

²¹⁵ *3.2. Reproducing kernel gradient smoothing approximation for effective stress
²¹⁶ and strain*

²¹⁷ In Galerkin meshfree formulation, the mid-plane of thin shell Ω is split by
²¹⁸ a set of integration cells Ω_C 's, $\cup_{C=1}^{n_e} \Omega_C \approx \Omega$, as shown in Fig. 2. With the
²¹⁹ inspiration of reproducing kernel smoothing framework, the Cartesian and co-
²²⁰ variant derivatives of displacement, $\mathbf{v}_{,\alpha}$ and $-\mathbf{v}_{,\alpha}|_\beta$, in strains $\varepsilon_{\alpha\beta}$, $\kappa_{\alpha\beta}$ are
²²¹ approximated by $(p-1)$ -th order polynomials in each integration cells. In inte-
²²² gration cell Ω_C , the approximated derivatives and strains denoted by $\mathbf{v}_{,\alpha}^h$, $\varepsilon_{\alpha\beta}^h$
²²³ and $-\mathbf{v}_{,\alpha}|_\beta$, $\kappa_{\alpha\beta}^h$ can be expressed by:

$$\mathbf{v}_{,\alpha}^h(\boldsymbol{\xi}) = \mathbf{q}^T(\boldsymbol{\xi}) \mathbf{d}_\alpha^\varepsilon, \quad \varepsilon_{\alpha\beta}^h(\boldsymbol{\xi}) = \mathbf{q}^T(\boldsymbol{\xi}) \frac{1}{2} (\mathbf{a}_\alpha \cdot \mathbf{d}_\beta^\varepsilon + \mathbf{a}_\beta \cdot \mathbf{d}_\alpha^\varepsilon) \quad (32)$$

$$-\mathbf{v}_{,\alpha}|_\beta(\boldsymbol{\xi}) = \mathbf{q}^T(\boldsymbol{\xi}) \mathbf{d}_{\alpha\beta}^\kappa, \quad \kappa_{\alpha\beta}^h(\boldsymbol{\xi}) = \mathbf{q}^T(\boldsymbol{\xi}) \mathbf{a}_3 \cdot \mathbf{d}_{\alpha\beta}^\kappa \quad (33)$$

²²⁴ where \mathbf{q} is the linear polynomial vector and has the following form:

$$\mathbf{q} = \{1, \xi^1, \xi^2\}^T \quad (34)$$

²²⁵ and the $\mathbf{d}_\alpha^\varepsilon$, $\mathbf{d}_{\alpha\beta}^\kappa$ are the corresponding coefficient vector tensors. For the con-
²²⁶ ciseness, the mixed usage of tensor and vector is introduced in this study. For
²²⁷ instance, the component of coefficient tensor vector $\mathbf{d}_{\alpha I}^\varepsilon$, $\mathbf{d}_\alpha^\varepsilon = \{\mathbf{d}_{\alpha I}^\varepsilon\}$, is a three
²²⁸ dimensional tensor, $\dim \mathbf{d}_{\alpha I}^\varepsilon = \dim \mathbf{v}$.

²²⁹ In order to meet the integration constraint of thin shell problem, the ap-
²³⁰ proximated stresses $N^{\alpha\beta h}$, $M^{\alpha\beta h}$ are assumed to be a similar form with strains,
²³¹ yields:

$$N^{\alpha\beta h}(\boldsymbol{\xi}) = \mathbf{q}^T(\boldsymbol{\xi}) \mathbf{a}^\alpha \cdot \mathbf{d}_N^\beta, \quad \mathbf{a}_\alpha N^{\alpha\beta h}(\boldsymbol{\xi}) = \mathbf{q}^T(\boldsymbol{\xi}) \mathbf{d}_N^\beta \quad (35)$$

$$M^{\alpha\beta h}(\boldsymbol{\xi}) = \mathbf{q}^T(\boldsymbol{\xi}) \mathbf{a}_3 \cdot \mathbf{d}_M^{\alpha\beta}, \quad \mathbf{a}_3 M^{\alpha\beta h}(\boldsymbol{\xi}) = \mathbf{q}^T(\boldsymbol{\xi}) \mathbf{d}_M^{\alpha\beta} \quad (36)$$

²³² substituting the approximations of Eqs. (22), (32), (33), (35), (36) into Eqs.
²³³ (21c), (21d) can express $\mathbf{d}_\beta^\varepsilon$ and $\mathbf{d}_{\alpha\beta}^\kappa$ by \mathbf{d} as:

$$\mathbf{d}_\beta^\varepsilon = \mathbf{G}^{-1} \left(\sum_{I=1}^{n_p} (\tilde{\mathbf{g}}_{\beta I} - \bar{\mathbf{g}}_{\beta I}) \mathbf{d}_I + \hat{\mathbf{g}}_\beta \right) \quad (37)$$

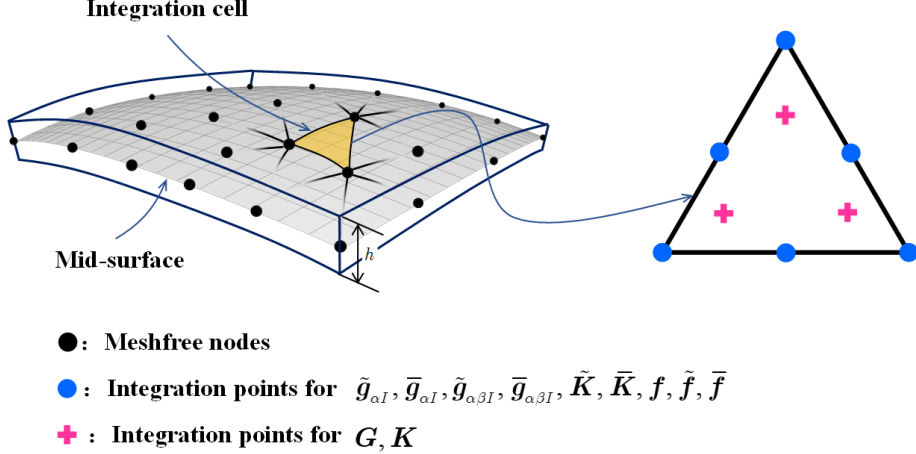


Figure 2: Integration scheme for Hu-Washizu weak form.

236

$$\mathbf{d}_{\alpha\beta}^\kappa = \mathbf{G}^{-1} \left(\sum_{I=1}^{n_p} (\tilde{\mathbf{g}}_{\alpha\beta I} - \bar{\mathbf{g}}_{\alpha\beta I}) \mathbf{d}_I + \hat{\mathbf{g}}_{\alpha\beta} \right) \quad (38)$$

237 with

$$\mathbf{G} = \int_{\Omega_C} \mathbf{q}^T \mathbf{q} d\Omega \quad (39)$$

238

$$\tilde{\mathbf{g}}_{\beta I} = \int_{\Gamma_C} \Psi_I \mathbf{q} n_\beta d\Gamma - \int_{\Omega_C} \Psi_I \mathbf{q}_{|\beta} d\Omega \quad (40a)$$

$$\bar{\mathbf{g}}_{\beta I} = \int_{\Gamma_C \cap \Gamma_v} \Psi_I \mathbf{q} n_\beta d\Gamma \quad (40b)$$

$$\hat{\mathbf{g}}_\beta = \int_{\Gamma_C \cap \Gamma_v} \mathbf{q} n_\beta \bar{\mathbf{v}} d\Gamma \quad (40c)$$

239

$$\begin{aligned} \tilde{\mathbf{g}}_{\alpha\beta I} &= \int_{\Gamma_C} \Psi_{I,\gamma} n^\gamma \mathbf{q} n_\alpha n_\beta d\Gamma - \int_{\Gamma_C} \Psi_I (\mathbf{q}_{|\beta} n_\alpha + (\mathbf{q} s_\alpha n_\beta)_{,\gamma} s^\gamma) d\Gamma \\ &\quad + [[\Psi_I \mathbf{q} s_\alpha n_\beta]]_{\mathbf{x} \in C_C} - \int_{\Omega_C} \Psi_I \mathbf{q}_{,\alpha|\beta} d\Omega \end{aligned} \quad (41a)$$

$$\begin{aligned} \bar{\mathbf{g}}_{\alpha\beta I} &= \int_{\Gamma_C \cap \Gamma_\theta} \Psi_{I,\gamma} n^\gamma \mathbf{q} n_\alpha n_\beta d\Gamma - \int_{\Gamma_C \cap \Gamma_v} \Psi_I (\mathbf{q}_{|\beta} n_\alpha + (\mathbf{q} s_\alpha n_\beta)_{,\gamma} s^\gamma) d\Gamma \\ &\quad + [[\Psi_I \mathbf{q} s_\alpha n_\beta]]_{\mathbf{x} \in C_C \cap C_v} \end{aligned} \quad (41b)$$

$$\begin{aligned} \hat{\mathbf{g}}_{\alpha\beta} &= \int_{\Gamma_C \cap \Gamma_\theta} \mathbf{q} n_\alpha n_\beta \bar{\mathbf{a}}_3 \bar{\mathbf{n}} d\Gamma - \int_{\Gamma_C \cap \Gamma_v} (\mathbf{q}_{|\beta} n_\alpha + (\mathbf{q} s_\alpha n_\beta)_{,\gamma} s^\gamma) \bar{\mathbf{v}} d\Gamma \\ &\quad + [[\mathbf{q} s_\alpha n_\beta \bar{\mathbf{v}}]]_{\mathbf{x} \in C_C \cap C_v} \end{aligned} \quad (41c)$$

²⁴⁰ where evaluations of $\mathbf{q}_{|\beta}$, $\mathbf{q}_{,\alpha|\beta}$ are detail in Appendix A. Further plugging Eqs.
²⁴¹ (37) and (38) back into Eqs. (32) and (33) respectively gives the final expression
²⁴² of $\mathbf{v}_{,\alpha}^h$, $\varepsilon_{\alpha\beta}^h$ and $-\mathbf{v}_{,\alpha\beta}^h$, $\kappa_{\alpha\beta}^h$ as:

$$\mathbf{v}_{,\alpha}^h = \sum_{I=1}^{n_p} (\tilde{\Psi}_{I,\alpha} - \bar{\Psi}_{I,\alpha}) \mathbf{d}_I + \mathbf{q}^T \mathbf{G}^{-1} \hat{\mathbf{g}}_\alpha \quad (42a)$$

$$\begin{aligned} \varepsilon_{\alpha\beta}^h &= \sum_{I=1}^{n_p} \frac{1}{2} (\mathbf{a}_\alpha \tilde{\Psi}_{I,\beta} + \mathbf{a}_\beta \tilde{\Psi}_{I,\alpha}) \cdot \mathbf{d}_I - \sum_{I=1}^{n_p} \frac{1}{2} (\mathbf{a}_\alpha \bar{\Psi}_{I,\beta} + \mathbf{a}_\beta \bar{\Psi}_{I,\alpha}) \cdot \mathbf{d}_I \\ &\quad + \mathbf{q}^T \mathbf{G}^{-1} \frac{1}{2} (\mathbf{a}_\alpha \cdot \hat{\mathbf{g}}_\beta + \mathbf{a}_\beta \cdot \hat{\mathbf{g}}_\alpha) \\ &= \tilde{\varepsilon}_{\alpha\beta}^h - \bar{\varepsilon}_{\alpha\beta}^h + \hat{\varepsilon}_{\alpha\beta}^h \end{aligned} \quad (42b)$$

$$-\mathbf{v}_{,\alpha}^h|_\beta = \sum_{I=1}^{n_p} (\tilde{\Psi}_{I,\alpha\beta} - \bar{\Psi}_{I,\alpha\beta}) \mathbf{d}_I + \mathbf{q}^T \mathbf{G}^{-1} \hat{\mathbf{g}}_{\alpha\beta} \quad (43a)$$

$$\begin{aligned} \kappa_{\alpha\beta}^h &= \sum_{I=1}^{n_p} \tilde{\Psi}_{I,\alpha\beta} \mathbf{a}_3 \cdot \mathbf{d}_I - \sum_{I=1}^{n_p} \bar{\Psi}_{I,\alpha\beta} \mathbf{a}_3 \cdot \mathbf{d}_I + \mathbf{q}^T \mathbf{G}^{-1} \mathbf{a}_3 \cdot \hat{\mathbf{g}}_{\alpha\beta} \\ &= \tilde{\kappa}_{\alpha\beta}^h - \bar{\kappa}_{\alpha\beta}^h + \hat{\kappa}_{\alpha\beta}^h \end{aligned} \quad (43b)$$

²⁴⁶ with

$$\begin{cases} \tilde{\varepsilon}_{\alpha\beta}^h = \sum_{I=1}^{n_p} \frac{1}{2} (\mathbf{a}_\alpha \tilde{\Psi}_{I,\beta} + \mathbf{a}_\beta \tilde{\Psi}_{I,\alpha}) \cdot \mathbf{d}_I = \sum_{I=1}^{n_p} \tilde{\varepsilon}_{\alpha\beta I} \cdot \mathbf{d}_I \\ \bar{\varepsilon}_{\alpha\beta}^h = \sum_{I=1}^{n_p} \frac{1}{2} (\mathbf{a}_\alpha \bar{\Psi}_{I,\beta} + \mathbf{a}_\beta \bar{\Psi}_{I,\alpha}) \cdot \mathbf{d}_I = \sum_{I=1}^{n_p} \bar{\varepsilon}_{\alpha\beta I} \cdot \mathbf{d}_I \\ \hat{\varepsilon}_{\alpha\beta}^h = \mathbf{q}^T \mathbf{G}^{-1} \frac{1}{2} (\mathbf{a}_\alpha \cdot \hat{\mathbf{g}}_\beta + \mathbf{a}_\beta \cdot \hat{\mathbf{g}}_\alpha) \end{cases} \quad (44)$$

$$\begin{cases} \tilde{\Psi}_{I,\alpha}(\boldsymbol{\xi}) = \mathbf{q}^T(\boldsymbol{\xi}) \mathbf{G}^{-1} \tilde{\mathbf{g}}_{\alpha I} \\ \bar{\Psi}_{I,\alpha}(\boldsymbol{\xi}) = \mathbf{q}^T(\boldsymbol{\xi}) \mathbf{G}^{-1} \bar{\mathbf{g}}_{\alpha I} \\ \tilde{\varepsilon}_{\alpha\beta I} = \frac{1}{2} (\mathbf{a}_\alpha \tilde{\Psi}_{I,\beta} + \mathbf{a}_\beta \tilde{\Psi}_{I,\alpha}) \\ \bar{\varepsilon}_{\alpha\beta I} = \frac{1}{2} (\mathbf{a}_\alpha \bar{\Psi}_{I,\beta} + \mathbf{a}_\beta \bar{\Psi}_{I,\alpha}) \end{cases} \quad (45)$$

$$\begin{cases} \tilde{\kappa}_{\alpha\beta}^h = \sum_{I=1}^{n_p} \tilde{\Psi}_{I,\alpha\beta} \mathbf{a}_3 \cdot \mathbf{d}_I = \sum_{I=1}^{n_p} \tilde{\kappa}_{\alpha\beta I} \cdot \mathbf{d}_I \\ \bar{\kappa}_{\alpha\beta}^h = \sum_{I=1}^{n_p} \bar{\Psi}_{I,\alpha\beta} \mathbf{a}_3 \cdot \mathbf{d}_I = \sum_{I=1}^{n_p} \bar{\kappa}_{\alpha\beta I} \cdot \mathbf{d}_I \\ \hat{\kappa}_{\alpha\beta}^h = \mathbf{q}^T \mathbf{G}^{-1} \mathbf{a}_3 \cdot \hat{\mathbf{g}}_{\alpha\beta} \end{cases} \quad (46)$$

249

$$\begin{cases} \tilde{\Psi}_{I,\alpha\beta}(\xi) = \mathbf{q}^T(\xi) \mathbf{G}^{-1} \tilde{\mathbf{g}}_{\alpha\beta I} \\ \bar{\Psi}_{I,\alpha\beta}(\xi) = \mathbf{q}^T(\xi) \mathbf{G}^{-1} \tilde{\mathbf{g}}_{\alpha\beta I} \\ \tilde{\kappa}_{\alpha\beta I} = \tilde{\Psi}_{I,\alpha\beta} \mathbf{a}_3 \\ \bar{\kappa}_{\alpha\beta I} = \bar{\Psi}_{I,\alpha\beta} \mathbf{a}_3 \end{cases} \quad (47)$$

250 It has to be noted that, referring to reproducing kernel gradient smoothing
 251 framework [26], $\tilde{\Psi}_{I,\alpha}$, $\tilde{\Psi}_{I,\alpha\beta}$ are actually the first and second order smoothed
 252 gradients in curvilinear coordinates. $\tilde{\mathbf{g}}_{\alpha I}$ and $\tilde{\mathbf{g}}_{\alpha\beta I}$ are the right hand side in-
 253 tegration constraints for first and second order gradients, then this formulation
 254 can meet the variational consistency for the second order polynomials. It should
 255 be known that, in curved model, the variational consistency for non-polynomial
 256 functions, like trigonometric functions, should be required for the polynomial
 257 solution. Even with high order polynomial variational consistency, the proposed
 258 formulation can not exactly reproduce the solution spanned by basis functions.
 259 However, the accuracy of reproducing kernel smoothed gradients is still better
 260 than traditional meshfree formulation. Numerical examples in the section below
 261 will provide better evidence to prove the accuracy of the reproducing kernel
 262 smoothed gradients.

²⁶³ **4. Naturally variational enforcement for essential boundary condi-**
²⁶⁴ **tions**

²⁶⁵ *4.1. Discrete equilibrium equations*

²⁶⁶ With the approximated effective stresses and strains, the last equation of
²⁶⁷ weak form Eq. (21e) becomes:

$$-\sum_{C=1}^{n_e} \sum_{I=1}^{n_p} \delta \mathbf{d}_I \cdot \left((\tilde{\mathbf{g}}_{\alpha I}^T - \bar{\mathbf{g}}_{\alpha I}^T) \mathbf{d}_N^\alpha + (\tilde{\mathbf{g}}_{\alpha\beta I}^T - \bar{\mathbf{g}}_{\alpha\beta I}^T) \mathbf{d}_M^{\alpha\beta} \right) = -\sum_{I=1}^{n_p} \delta d_I \cdot \mathbf{f}_I \quad (48)$$

²⁶⁸ where \mathbf{f}_I 's are the components of the traditional force vector:

$$\mathbf{f}_I = \int_{\Gamma_t} \Psi_I \bar{\mathbf{t}} d\Gamma - \int_{\Gamma_M} \Psi_{I,\gamma} n^\gamma \bar{M}_{\mathbf{n}\mathbf{n}} d\Gamma + [[\Psi_I \mathbf{a}_3 \bar{P}]]_{\mathbf{x} \in C_P} + \int_{\Omega} \Psi_I \bar{\mathbf{b}} d\Omega \quad (49)$$

²⁶⁹ The left side of Eq. (48) can be simplified using the following steps. For clarity,
²⁷⁰ the derivation of first term in Eq. (48) taken as an example is given by:

$$\begin{aligned} \sum_{I=1}^{n_p} \delta \mathbf{d}_I \cdot \tilde{\mathbf{g}}_{\alpha I}^T \mathbf{d}_N^\alpha &= \sum_{I=1}^{n_p} \delta \mathbf{d}_I \cdot (\mathbf{G}^{-1} \tilde{\mathbf{g}}_{\alpha I})^T \mathbf{G} \mathbf{d}_N^\alpha \\ &= \int_{\Omega_C} \sum_{I=1}^{n_p} \delta \mathbf{d}_I \cdot (\mathbf{q}^T \mathbf{G}^{-1} \tilde{\mathbf{g}}_{\alpha I})^T \mathbf{q}^T \mathbf{d}_N^\alpha d\Omega \\ &= \int_{\Omega_C} \sum_{I=1}^{n_p} \delta \mathbf{d}_I \cdot \mathbf{a}_\beta (\mathbf{q}^T \mathbf{G}^{-1} \tilde{\mathbf{g}}_{\alpha I})^T N^{\alpha\beta h} d\Omega \\ &= \int_{\Omega_C} \delta \hat{\varepsilon}_{\alpha\beta}^h N^{\alpha\beta h} d\Omega \end{aligned} \quad (50)$$

²⁷¹ following the above procedure and including the weak form of Eqs. (21a), (21b),
²⁷² the left side of Eq. (48) in Ω_C becomes:

$$\begin{aligned}
& \sum_{I=1}^{n_p} \delta \mathbf{d}_I \cdot \left((\tilde{\mathbf{g}}_{\alpha I}^T - \bar{\mathbf{g}}_{\alpha I}^T) \mathbf{d}_N^\alpha + (\tilde{\mathbf{g}}_{\alpha \beta I}^T - \bar{\mathbf{g}}_{\alpha \beta I}^T) \mathbf{d}_M^{\alpha \beta} \right) \\
& = \int_{\Omega_C} ((\delta \tilde{\varepsilon}_{\alpha \beta}^h - \delta \bar{\varepsilon}_{\alpha \beta}^h) N^{\alpha \beta h} + (\delta \tilde{\kappa}_{\alpha \beta}^h - \delta \bar{\kappa}_{\alpha \beta}^h) M^{\alpha \beta h}) d\Omega \\
& = \int_{\Omega_C} (\delta \tilde{\varepsilon}_{\alpha \beta}^h - \delta \bar{\varepsilon}_{\alpha \beta}^h) h C^{\alpha \beta \gamma \eta} \varepsilon_{\gamma \eta}^h + (\delta \tilde{\kappa}_{\alpha \beta}^h - \delta \bar{\kappa}_{\alpha \beta}^h) \frac{h^3}{12} C^{\alpha \beta \gamma \eta} \kappa_{\gamma \eta}^h \\
& = \int_{\Omega_C} \delta \tilde{\varepsilon}_{\alpha \beta}^h h C^{\alpha \beta \gamma \eta} \tilde{\varepsilon}_{\gamma \eta}^h d\Omega + \int_{\Omega_C} \delta \tilde{\kappa}_{\alpha \beta}^h \frac{h^3}{12} C^{\alpha \beta \gamma \eta} \tilde{\kappa}_{\gamma \eta}^h d\Omega \\
& - \int_{\Omega_C} \delta \tilde{\varepsilon}_{\alpha \beta}^h h C^{\alpha \beta \gamma \eta} \bar{\varepsilon}_{\gamma \eta}^h d\Omega - \int_{\Omega_C} \delta \bar{\varepsilon}_{\alpha \beta}^h h C^{\alpha \beta \gamma \eta} \tilde{\varepsilon}_{\gamma \eta}^h d\Omega \\
& - \int_{\Omega_C} \delta \tilde{\kappa}_{\alpha \beta}^h \frac{h^3}{12} C^{\alpha \beta \gamma \eta} \bar{\kappa}_{\gamma \eta}^h d\Omega - \int_{\Omega_C} \delta \bar{\kappa}_{\alpha \beta}^h \frac{h^3}{12} C^{\alpha \beta \gamma \eta} \tilde{\kappa}_{\gamma \eta}^h d\Omega \\
& + \int_{\Omega_C} \delta \bar{\varepsilon}_{\alpha \beta}^h h C^{\alpha \beta \gamma \eta} \bar{\varepsilon}_{\gamma \eta}^h d\Omega + \int_{\Omega_C} \delta \bar{\kappa}_{\alpha \beta}^h \frac{h^3}{12} C^{\alpha \beta \gamma \eta} \bar{\kappa}_{\gamma \eta}^h d\Omega \\
& + \int_{\Omega_C} (\delta \tilde{\varepsilon}_{\alpha \beta}^h - \delta \bar{\varepsilon}_{\alpha \beta}^h) h C^{\alpha \beta \gamma \eta} \hat{\varepsilon}_{\gamma \eta}^h d\Omega + \int_{\Omega_C} (\delta \tilde{\kappa}_{\alpha \beta}^h - \delta \bar{\kappa}_{\alpha \beta}^h) \frac{h^3}{12} C^{\alpha \beta \gamma \eta} \hat{\kappa}_{\gamma \eta}^h d\Omega
\end{aligned} \tag{51}$$

²⁷³ on further substituting Eqs. (44) and (46) into above equation gives the final
²⁷⁴ discrete equilibrium equations, respectively:

$$(\mathbf{K} + \tilde{\mathbf{K}} + \bar{\mathbf{K}}) \mathbf{d} = \mathbf{f} + \tilde{\mathbf{f}} + \bar{\mathbf{f}} \tag{52}$$

²⁷⁵ where

$$\mathbf{K}_{IJ} = \int_{\Omega} \tilde{\varepsilon}_{\alpha \beta I} h C^{\alpha \beta \gamma \eta} \tilde{\varepsilon}_{\gamma \eta J} d\Omega + \int_{\Omega} \tilde{\kappa}_{\alpha \beta I} \frac{h^3}{12} C^{\alpha \beta \gamma \eta} \tilde{\kappa}_{\alpha \beta J} d\Omega \tag{53}$$

²⁷⁶

$$\begin{aligned}
\tilde{\mathbf{K}}_{IJ} = & - \int_{\Gamma_v} (\Psi_I \tilde{\mathbf{T}}_{NJ} + \tilde{\mathbf{T}}_{NJ} \Psi_J) d\Gamma \\
& + \int_{\Gamma_\theta} (\Psi_{I,\gamma} n^\gamma \mathbf{a}_3 \tilde{\mathbf{M}}_{nnJ} + \mathbf{a}_3 \tilde{\mathbf{M}}_{nnI} \Psi_{I,\gamma} n^\gamma) d\Gamma \\
& + ([[\Psi_I \mathbf{a}_3 \tilde{\mathbf{P}}_J]] + [[\tilde{\mathbf{P}}_I \mathbf{a}_3 \Psi_J]])_{\mathbf{x} \in C_v}
\end{aligned} \tag{54a}$$

$$\tilde{\mathbf{f}}_I = - \int_{\Gamma_v} \tilde{\mathbf{T}}_{NI} \cdot \bar{\mathbf{v}} d\Gamma + \int_{\Gamma_\theta} \tilde{\mathbf{M}}_{nnI} \bar{\theta}_n d\Gamma + [[\tilde{\mathbf{P}}_I \mathbf{a}_3 \cdot \bar{\mathbf{v}}]]_{\mathbf{x} \in C_v} \tag{54b}$$

²⁷⁷

$$\bar{\mathbf{K}}_{IJ} = - \int_{\Gamma_v} \bar{\mathbf{T}}_{MI} \Psi_J d\Gamma + \int_{\Gamma_\theta} \mathbf{a}_3 \bar{\mathbf{M}}_{nnI} \Psi_{J,\gamma} n^\gamma d\Gamma + [[\bar{\mathbf{P}}_I \mathbf{a}_3 \Psi_J]]_{\mathbf{x} \in C_v} \tag{55a}$$

$$\bar{\mathbf{f}}_I = - \int_{\Gamma_v} \bar{\mathbf{T}}_{MI} \cdot \bar{\mathbf{v}} d\Gamma + \int_{\Gamma_\theta} \bar{\mathbf{M}}_{nnI} \bar{\theta}_n d\Gamma + [[\bar{\mathbf{P}}_I \mathbf{a}_3 \cdot \bar{\mathbf{v}}]]_{\mathbf{x} \in C_v} \tag{55b}$$

278 The detailed derivations of Eqs (53)-(55) are listed in the Appendix B. As
 279 shown in these equations, Eq. (53) is the conventional stiffness matrix evaluated
 280 by smoothed gradients $\tilde{\Psi}_{I,\alpha}$, $\tilde{\Psi}_{I,\alpha}|_{\beta}$, and the Eqs. (54) and (55) contribute for
 281 the enforcement of essential boundary. It should be mentioned that, in accord-
 282 ance with reproducing kernel smoothed gradient framework, the integration
 283 scheme of Eqs. (53-55) should be aligned with the those used in the construc-
 284 tion of smoothed gradients. The integration scheme used for proposed method
 285 is shown in Fig. 2, in which the total number of the blue circular integration
 286 points has been optimized from a global point of view, aiming to reduce the com-
 287 putation of traditional meshfree shape functions and its first order derivatives.
 288 In contrast, for assembly stiffness matrix \mathbf{K} , the low order Gauss integration
 289 rule is suitable to ensure the accuracy due to the inherently variational consis-
 290 tency in smoothed gradients. The detailed positions and weight of integration
 291 points and the efficiency demonstration of this optimized integration scheme
 292 can be found in [26, 32] With a close look at Eqs. (54) and (55), the proposed
 293 approach for enforcing essential boundary conditions show an identical struc-
 294 ture with traditional Nitsche’s method, both have the consistent and stabilized
 295 terms. So, the next subsection will review the Nitsche’s method and compare
 296 it with the proposed method.

297 *4.2. Comparison with Nitsche’s method*

298 The Nitsche’s method for enforcing essential boundaries can be regarded as a
 299 combination of Lagrangian multiplier method and penalty method, in which the
 300 Lagrangian multiplier is represented by the approximated displacement. The
 301 corresponding total potential energy functional Π_P is given by:

$$\begin{aligned}
 \Pi_P(\mathbf{v}) = & \int_{\Omega} \frac{1}{2} \varepsilon_{\alpha\beta} N^{\alpha\beta} d\Omega + \int_{\Omega} \frac{1}{2} \kappa_{\alpha\beta} M^{\alpha\beta} d\Omega \\
 & - \int_{\Gamma_t} \mathbf{v} \cdot \bar{\mathbf{t}} d\Gamma + \int_{\Gamma_M} \mathbf{v}_{,\gamma} n^{\gamma} \mathbf{a}_3 M_{\mathbf{n}\mathbf{n}} d\Gamma + (\mathbf{v} \cdot \mathbf{a}_3 P)_{\mathbf{x} \in C_P} - \int_{\Omega} \mathbf{v} \cdot \bar{\mathbf{b}} d\Omega \\
 & - \underbrace{\int_{\Gamma_v} \mathbf{t} \cdot (\mathbf{v} - \bar{\mathbf{v}}) d\Gamma + \int_{\Gamma_{\theta}} M_{\mathbf{n}\mathbf{n}} (\theta_{\mathbf{n}} - \bar{\theta}_{\mathbf{n}}) d\Gamma + (P \mathbf{a}_3 \cdot (\mathbf{v} - \bar{\mathbf{v}}))_{\mathbf{x} \in C_v}}_{\text{consistent term}} \quad (56) \\
 & + \underbrace{\sum_{i=1}^3 \frac{\alpha_{vi}}{2} \int_{\Gamma_v} \mathbf{v} \cdot \mathbf{v} d\Gamma + \frac{\alpha_{\theta}}{2} \int_{\Gamma_{\theta}} \theta_{\mathbf{n}}^2 d\Gamma + \frac{\alpha_C}{2} (\mathbf{v} \cdot \mathbf{a}_3)_{\mathbf{x} \in C_v}^2}_{\text{stabilized term}}
 \end{aligned}$$

302 where the consistent term generated from the Lagrangian multiplier method
 303 contributes to enforce the essential boundary, and meet the variational con-
 304 sistency condition. However, the consistent term can not always ensure the
 305 coercivity of stiffness, so the penalty method is introduced to serve as a sta-
 306 bilized term, in which α_{vi} ’s, α_{θ} and α_C are experimental artificial parameters
 307 in penalty method. With a standard variational argument, the corresponding

³⁰⁸ weak form can be stated as:

$$\begin{aligned}
\delta\Pi_P(\mathbf{v}) &= \int_{\Omega} \delta\varepsilon_{\alpha\beta} N^{\alpha\beta} d\Omega + \int_{\Omega} \delta\kappa_{\alpha\beta} M^{\alpha\beta} d\Omega \\
&\quad - \int_{\Gamma_t} \delta\mathbf{v} \cdot \bar{\mathbf{t}} d\Gamma + \int_{\Gamma_M} \delta\mathbf{v}_{,\gamma} n^\gamma \mathbf{a}_3 M_{\mathbf{n}\mathbf{n}} d\Gamma + (\delta\mathbf{v} \cdot \mathbf{a}_3 P)_{\mathbf{x} \in C_P} - \int_{\Omega} \delta\mathbf{v} \cdot \bar{\mathbf{b}} d\Omega \\
&\quad - \int_{\Gamma_v} \delta\mathbf{v} \cdot \mathbf{t} d\Gamma + \int_{\Gamma_\theta} \delta\theta_{\mathbf{n}} M_{\mathbf{n}\mathbf{n}} d\Gamma + (\mathbf{v} \cdot \mathbf{a}_3 P)_{\mathbf{x} \in C_v} \\
&\quad - \int_{\Gamma_v} \delta\mathbf{t} \cdot (\mathbf{v} - \bar{\mathbf{v}}) d\Gamma + \int_{\Gamma_\theta} \delta M_{\mathbf{n}\mathbf{n}} (\theta_{\mathbf{n}} - \bar{\theta}_{\mathbf{n}}) d\Gamma + (\delta P \mathbf{a}_3 \cdot (\mathbf{v} - \bar{\mathbf{v}}))_{\mathbf{x} \in C_v} \\
&\quad + \sum_{i=1}^3 \alpha_{vi} \int_{\Gamma_v} (\delta\mathbf{v} \cdot \mathbf{a}_i) (\mathbf{a}_i \cdot \mathbf{v}) d\Gamma + \alpha_\theta \int_{\Gamma_\theta} \delta\theta_{\mathbf{n}} \theta_{\mathbf{n}} d\Gamma + \alpha_C (\delta\mathbf{v} \cdot \mathbf{a}_3 \mathbf{a}_3 \cdot \mathbf{v})_{\mathbf{x} \in C_v} \\
&= 0
\end{aligned} \tag{57}$$

³⁰⁹ Further invoking the conventional reproducing kernel approximation of Eq. (22)
³¹⁰ leads to the following discrete equilibrium equations:

$$\sum_{J=1}^{n_p} (\mathbf{K}_{IJ} + \mathbf{K}_{IJ}^c + \mathbf{K}_{IJ}^s) \mathbf{d}_J = \mathbf{f}_I + \mathbf{f}^c + \mathbf{f}^s \tag{58}$$

³¹¹ where the stiffness \mathbf{K}_{IJ} is identical with Eq. (53). \mathbf{K}_{IJ}^c and \mathbf{K}_{IJ}^s are the stiffness
³¹² matrices for consistent and stabilized terms, respectively, and have the following
³¹³ form:

$$\begin{aligned}
\mathbf{K}_{IJ}^c &= - \int_{\Gamma_v} (\Psi_I \mathbf{T}_{NJ} + \mathbf{T}_{NJ} \Psi_J) d\Gamma \\
&\quad + \int_{\Gamma_\theta} (\Psi_{I,\gamma} n^\gamma \mathbf{a}_3 M_{\mathbf{n}\mathbf{n},J} + \mathbf{a}_3 M_{\mathbf{n}\mathbf{n},I} \Psi_{I,\gamma} n^\gamma) d\Gamma \\
&\quad + ([[\Psi_I \mathbf{a}_3 \mathbf{P}_J]] + [[\mathbf{P}_I \mathbf{a}_3 \Psi_J]])_{\mathbf{x} \in C_v}
\end{aligned} \tag{59a}$$

$$\mathbf{f}_I^c = - \int_{\Gamma_v} \mathbf{T}_I \cdot \bar{\mathbf{v}} d\Gamma + \int_{\Gamma_\theta} \mathbf{M}_{\mathbf{n}\mathbf{n},I} \bar{\theta}_{\mathbf{n}} d\Gamma + [[\mathbf{P}_I \mathbf{a}_3 \cdot \bar{\mathbf{v}}]]_{\mathbf{x} \in C_v} \tag{59b}$$

³¹⁴

$$\mathbf{K}_{IJ}^s = \boldsymbol{\alpha}_v \int_{\Gamma_v} \Psi_I \Psi_J d\Gamma + \alpha_\theta \int_{\Gamma_\theta} \Psi_{I,\eta} n^\eta \mathbf{a}_3 \mathbf{a}_3 n^\gamma \Psi_{J,\gamma} d\Gamma + \alpha_C [[\Psi_I \mathbf{a}_3 \mathbf{a}_3 \Psi_J]]_{\mathbf{x} \in C_v} \tag{60a}$$

$$\mathbf{f}_I^s = \boldsymbol{\alpha}_v \int_{\Gamma_v} \Psi_I \bar{\mathbf{v}} d\Gamma + \alpha_\theta \int_{\Gamma_\theta} \Psi_{I,\eta} n^\eta \mathbf{a}_3 \bar{\theta}_{\mathbf{n}} d\Gamma + \alpha_C [[\Psi_I \mathbf{a}_3 \mathbf{a}_3 \cdot \bar{\mathbf{v}}]]_{\mathbf{x} \in C_v} \tag{60b}$$

³¹⁵ with

$$\boldsymbol{\alpha}_v = \begin{bmatrix} \alpha_{v1} & 0 & 0 \\ 0 & \alpha_{v2} & 0 \\ 0 & 0 & \alpha_{v3} \end{bmatrix} \tag{61}$$

316 On comparing with the consistent terms of Eqs. (54) and (59), the expres-
317 sions were almost identical, the major difference is that the higher order deriva-
318 tives of shape functions have been replaced by smoothed gradients. Owing to
319 the reproducing kernel framework, the construction of smoothed gradients only
320 concerned about the computation of traditional meshfree shape functions and
321 their first order derivatives, which avoid the costly computation of higher order
322 derivatives. Moreover, the stabilized terms in Eq. (60) employs the penalty
323 method with big enough artificial parameters to ensure the coercivity of stiff-
324 ness. And the optimal values of these artificial parameters are proportional to
325 the grid size of discrete model that can be represented by support size in mesh-
326 free approximation, where the $\alpha_{v\alpha} \propto s^{-1}$, $\alpha_{v3} \propto s^{-3}$, $\alpha_\theta \propto s^{-1}$, $\alpha_C \propto s^{-2}$ [30],
327 and $s = \min\{s_{\alpha I}\}$. In contrast, the stabilized term of Eq. (55) naturally exists
328 in its weak form, and can stabilize the result without considering any artificial
329 parameters.

330 **5. Numerical examples**

331 The suggested method, which uses Nitsche's method, the consistent repro-
 332 ducing kernel gradient smoothing integration scheme (RKGSI), and the non-
 333 consistent Gauss integration scheme (GI) with penalty method, as well as the
 334 proposed Hu-Washizu formulation (HW) to enforce the necessary boundary con-
 335 ditions, is validated in this section through several examples. A normalized
 336 support size of 2.5 is used for all the methods to ensure the requirement of
 337 quadratic base meshfree approximation. To eliminate the influence of integra-
 338 tion, the Gauss integration scheme uses 6 Gauss points for domain integration
 339 and 3 points for boundary integration, so as to maintain the same integration
 340 accuracy between domain and boundaries. Moreover, the number of integra-
 341 tion points are identical between the Gauss and RKGSI schemes. The error
 342 estimates of displacement (L_2 -Error) and energy (H_e -Error) is used here:

$$L_2\text{-Error} = \frac{\sqrt{\int_{\Omega}(\mathbf{v} - \mathbf{v}^h) \cdot (\mathbf{v} - \mathbf{v}^h) d\Omega}}{\sqrt{\mathbf{v} \cdot \mathbf{v}}}$$

$$H_e\text{-Error} = \frac{\sqrt{\int_{\Omega}((\varepsilon_{\alpha\beta} - \varepsilon_{\alpha\beta}^h)(N^{\alpha\beta} - N^{\alpha\beta h}) + \int_{\Omega}(\kappa_{\alpha\beta} - \kappa_{\alpha\beta}^h)(M^{\alpha\beta} - M^{\alpha\beta h})) d\Omega}}{\sqrt{\int_{\Omega}(\varepsilon_{\alpha\beta} N^{\alpha\beta} + \kappa_{\alpha\beta} M^{\alpha\beta}) d\Omega}}$$
(62)

343 *5.1. Patch tests*

344 The linear and quadratic patch tests for flat and curved thin shells are firstly
 345 studied to verify the variational consistency of the proposed method. As shown
 346 in Fig. 3, the flat and curved models are depicted by an identical parametric
 347 domain $\Omega = (0, 1) \otimes (0, 1)$, where the cylindrical coordinate system with radius
 348 $R = 1$ is employed to describe the curved model, and the whole domain Ω
 349 is discretized by the 165 meshfree nodes. The artificial parameters of $\alpha_v =$
 350 10^5 , $\alpha_\theta = 10^3$, $\alpha_C = 10^5$ and $\alpha_v = 10^9$, $\alpha_\theta = 10^9$, $\alpha_C = 10^9$ are used for Nitsche's
 351 method and penalty method respectively. All the boundaries are enforced as
 352 essential boundary conditions with the following manufactured exact solution:

$$\mathbf{v} = \begin{cases} (\xi^1 + 2\xi^2)^n \\ (3\xi^1 + 4\xi^2)^n \\ (5\xi^1 + 6\xi^2)^n \end{cases}, \quad n = \begin{cases} 1 & \text{Linear patch test} \\ 2 & \text{Quadratic patch test} \end{cases}$$
(63)

353 Table 1 lists the L_2 - and H_e -Error results of patch test with flat model, where
 354 the RKGSI scheme with variational consistent essential boundary enforcement,
 355 i.e. RKGSI-Nitsche and RKGSI-HW, can pass the linear and quadratic patch
 356 test. In contrast, the RKGSI-Penalty cannot pass the patch test since the
 357 Penalty method is unable to ensure the variational consistency. Due to the
 358 loss of variational consistency condition, even with Nitsche's method, Gauss
 359 meshfree formulations show noticeable errors. Table 2 shows the results for
 360 curved model, which indicated that all the considered methods cannot pass the

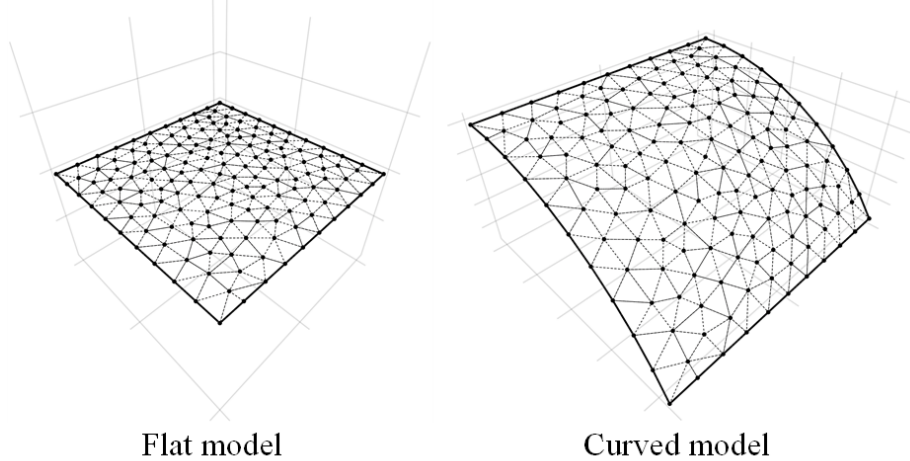


Figure 3: Meshfree discretization for patch test

patch test. This is mainly because the proposed smoothed gradient of Eqs. (35) and (36) could not exactly reproduce the non-polynomial membrane and bending stress. However, the RKGSI-HW and RKGSI-Nitsche methods also provide better accuracy compared to others due to the fulfillment of first second-order variational consistency. And, even only with local variational consistency, the RKGSI-Penalty obtained a better result than traditional Gauss scheme. Meanwhile, the bending moment contours of M^{12} are listed in Fig. 4, which further verify that the proposed method provided a satisfactory result compared to exact solution. On the other hand, the RKGSI-Penalty and the conventional Gauss meshfree formulations showed errors.

Table 1: Results of patch test for flat model.

	Linear patch test		Quadratic patch test	
	L_2 -Error	H_e -Error	L_2 -Error	H_e -Error
GI-Penalty	$4.45E - 4$	$1.35E - 2$	$2.01E - 3$	$1.63E - 2$
GI-Nitsche	$4.51E - 4$	$1.42E - 2$	$1.22E - 3$	$1.68E - 2$
RKGSI-Penalty	$3.64E - 9$	$6.77E - 8$	$4.54E - 9$	$6.57E - 8$
RKGSI-Nitsche	$3.31E - 12$	$1.34E - 11$	$5.98E - 12$	$1.21E - 11$
RKGSI-HR	$6.67E - 13$	$1.50E - 11$	$1.07E - 12$	$1.26E - 11$

5.2. Scordelis-Lo roof

This example considers the classical Scordelis-Lo roof problem, as depicted in Fig. 5. The cylindrical roof has dimensions $R = 25$, $L = 50$, $h = 0.25$, Young's modulus $E = 4.32 \times 10^8$ and Poisson's ratio $\nu = 0.0$. The entire roof

Table 2: Results of patch test for cylindrical model.

	Linear patch test		Quadratic patch test	
	L_2 -Error	H_e -Error	L_2 -Error	H_e -Error
GI-Penalty	$3.79E - 4$	$1.30E - 2$	$1.74E - 3$	$1.37E - 2$
GI-Nitsche	$4.04E - 4$	$1.42E - 2$	$1.15E - 3$	$1.49E - 2$
RKGSI-Penalty	$1.47E - 4$	$5.39E - 3$	$2.26E - 4$	$2.09E - 3$
RKGSI-Nitsche	$2.41E - 6$	$7.37E - 5$	$2.47E - 6$	$2.89E - 5$
RKGSI-HR	$4.28E - 6$	$1.30E - 4$	$9.69E - 6$	$2.41E - 4$

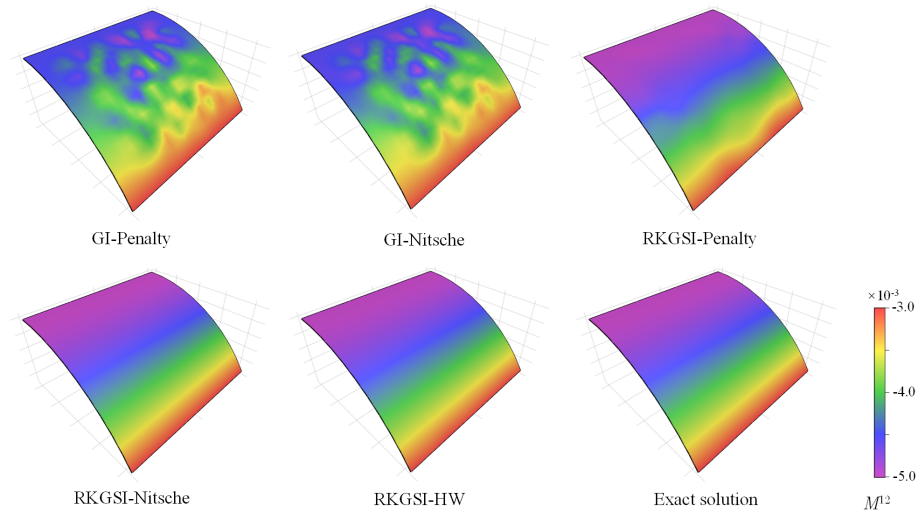


Figure 4: Contour plots of M^{12} for curved shell patch test.

is subjected to an uniform body force of $b_z = -90$, with the straight edges remainning free and the the curved edges are enforced by $v_x = v_z = 0$.

Due to the symmetry, only a quadrant of the model is considered for meshfree analysis, which is discretized by the 11×16 , 13×20 , 17×24 and 19×28 meshfree nodes, as listed in Fig. 6. The comparison of the displacement in z -direction at node A , v_{A3} , is used as the investigated quantity, with the reference value 0.3006 given by [33]. Firstly, Fig. 7 presents a sensitivity study for the artificial parameters of α_{vi} 's and α_θ 's in the RKGSI meshfree formulations with Nitsche's method and penalty method, where all of the parameters are scaled by the support size as, $\alpha_{v\alpha} = s^{-1}\bar{\alpha}_v$, $\alpha_{v3} = s^{-3}\bar{\alpha}_v$ and $\alpha_\theta = s^{-1}\bar{\alpha}_\theta$. For a better comparison, the result of proposed RKGSI-HW is also listed in this figure. The results of Fig. 7 revealed, Nitsche's method observed less artificial sensitivity. However, both the methods cannot trivially determine the optimal values of the artificial parameters. The optimal artificial parameters from Fig. 7 are adopted for the convergence study in Fig. 8. The convergence result showed

³⁹⁰ that the RKGSI get satisfactory results while the traditional Gauss methods
³⁹¹ demonstrated noticeable errors.

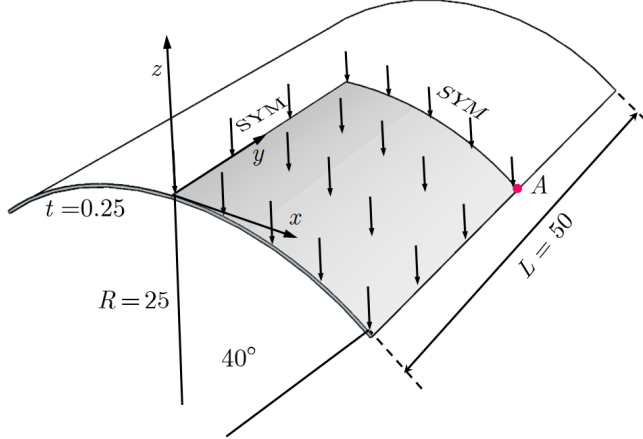


Figure 5: Description of Scordelis-Lo roof problem.

³⁹² *5.3. Pinched Hemispherical shell*

³⁹³ Consider the hemispherical shell shown in Fig. 9, which is loaded at four
³⁹⁴ points $P = \pm 2$ at 90° interval at its bottom. The hemispherical shell has an
³⁹⁵ radius $R = 10$, thickness $h = 0.04$, Young's modulus $E = 6.825 \times 10^7$ and
³⁹⁶ Poisson's ratio $\nu = 0.3$.

³⁹⁷ Due to symmetry, only quadrant model, where the 16×16 , 24×24 , 32×32
³⁹⁸ and 40×40 meshfree nodes have been discretized as shown in Fig. (10), was con-
³⁹⁹ sidered. The quantity under investigation for convergence is the displacement
⁴⁰⁰ at x -direction on point A , v_{A1} . Fig. 11 displays the corresponding convergence
⁴⁰¹ results, indicating the RKGSI scheme performed significantly better compared
⁴⁰² to the GI meshfree formulation. Meanwhile, the efficiency comparison for this
⁴⁰³ problem is also shown in Fig. 12, in which the CPU time for assembly and
⁴⁰⁴ calculation of shape functions are considered. Fig. 12(a) indicates that the
⁴⁰⁵ RKGSI scheme observed high efficiency in assembly. This is due to the vari-
⁴⁰⁶ ational inconsistent Gauss meshfree formulation which require more Gaussian
⁴⁰⁷ points to get satisfactory results. Fig. 12(b) lists the CPU time spent on enforc-
⁴⁰⁸ ing essential boundary conditions for the penalty method, Nitsche's method and
⁴⁰⁹ proposed HW method. The results highlighted that the proposed HW method
⁴¹⁰ consumed comparable CPU time in assembly compared to Nitsche's method.
⁴¹¹ However, less time was spent to calculate the shape functions. Since both the
⁴¹² HW method and penalty method were developed considering the shape func-
⁴¹³ tions first order derivatives. For this reason, both the methods shared an almost
⁴¹⁴ identical time in computing the shape functions.

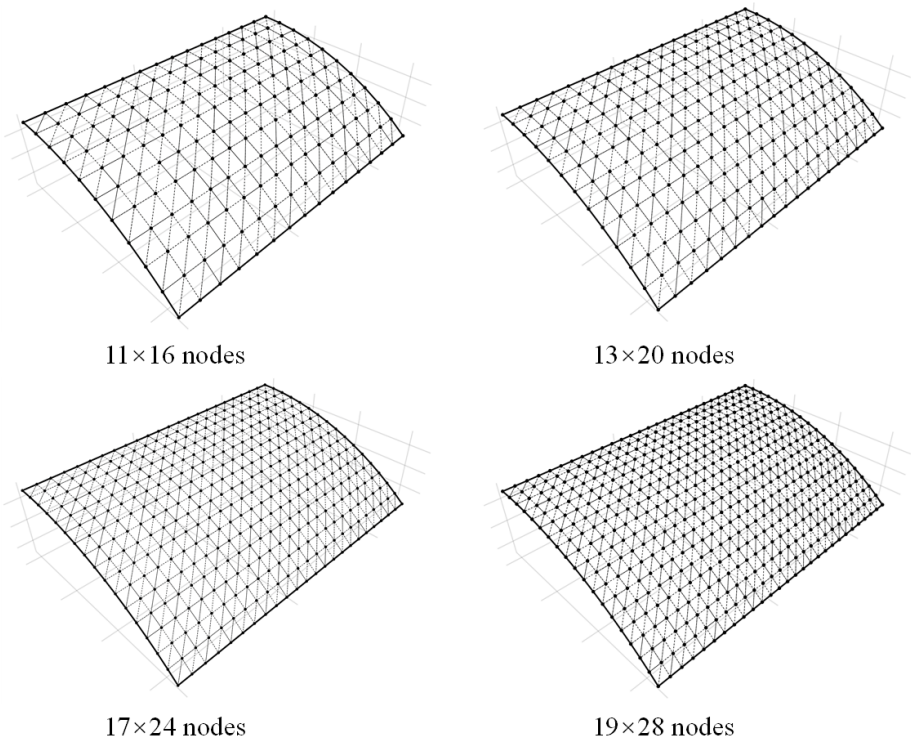
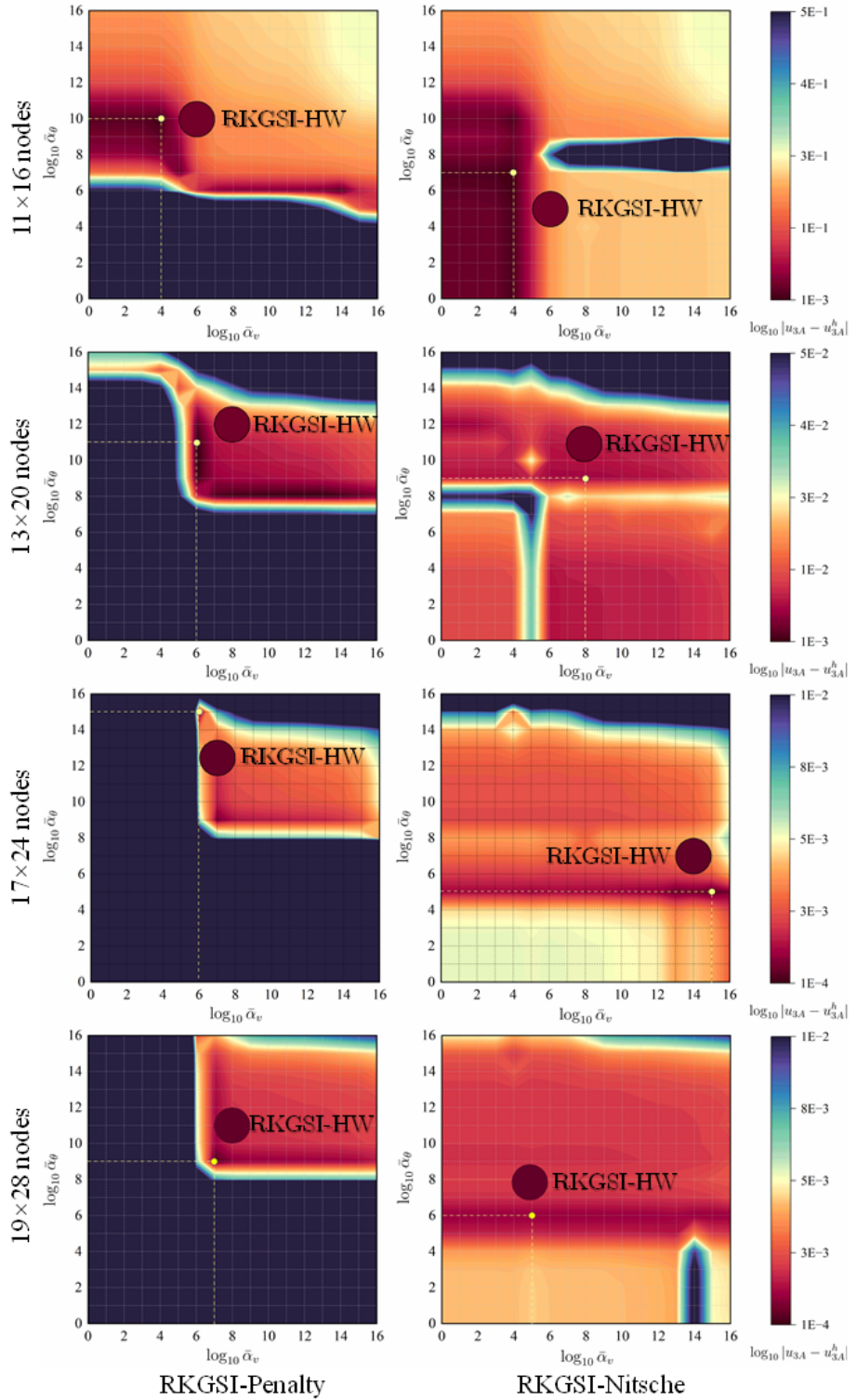


Figure 6: Meshfree discretizations for Scordelis-Lo roof problem.

Figure 7: Sensitivity comparison of α_v and α_θ for Scordelis-Lo problem.

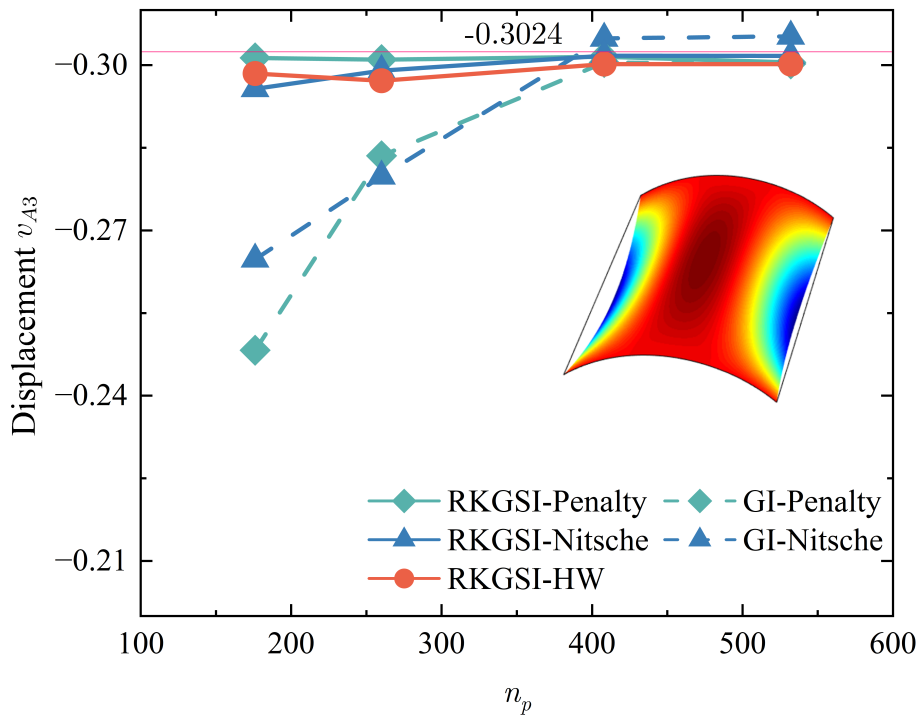


Figure 8: Displacement convergence for Scordelis-Lo roof problem.

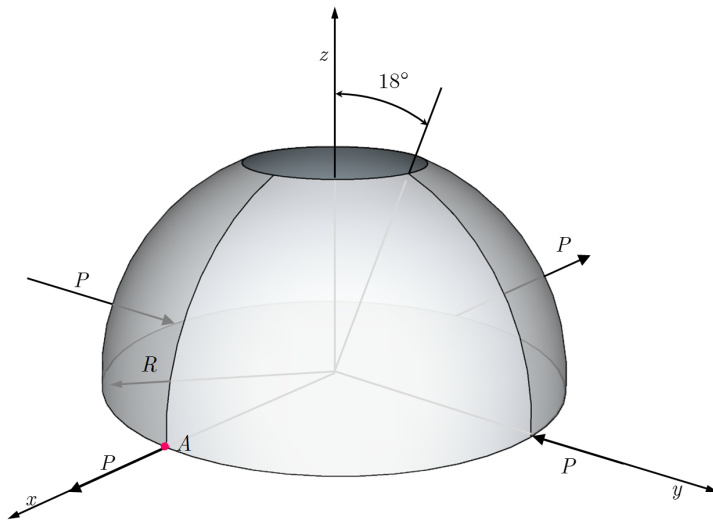


Figure 9: Description of pinched hemispherical shell problem.

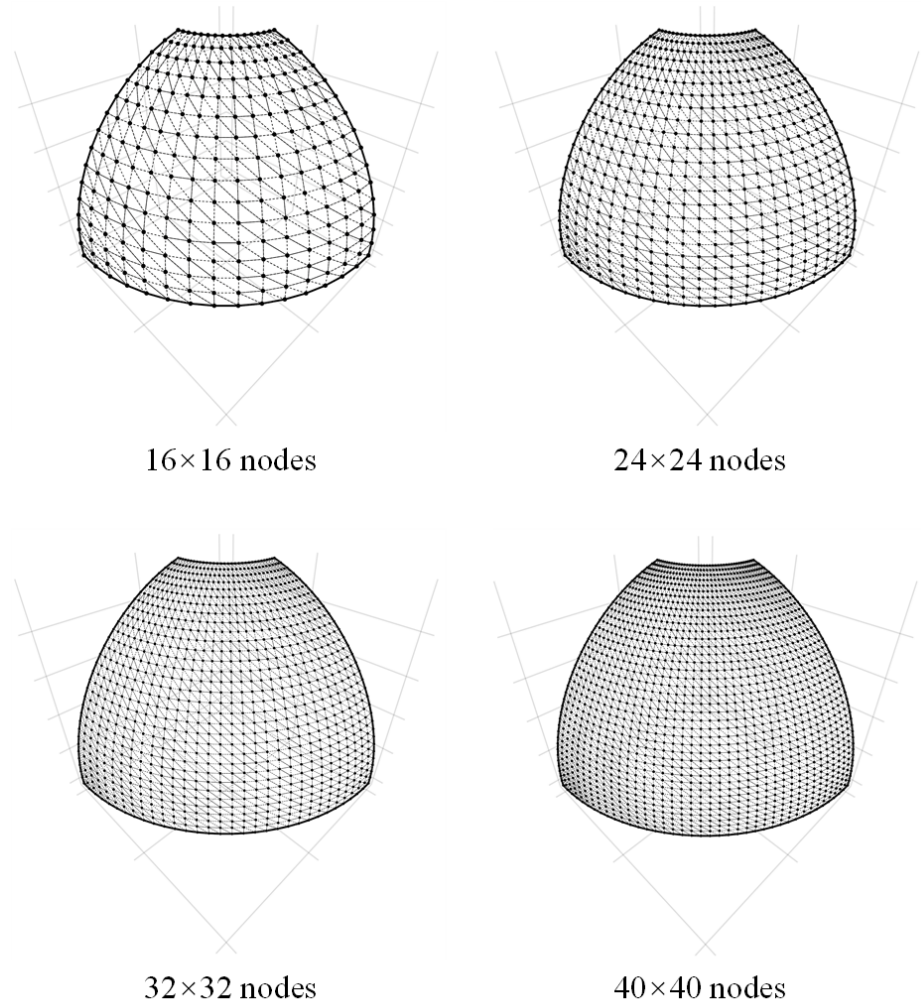


Figure 10: Meshfree discretizations for pinched hemispherical shell problem.

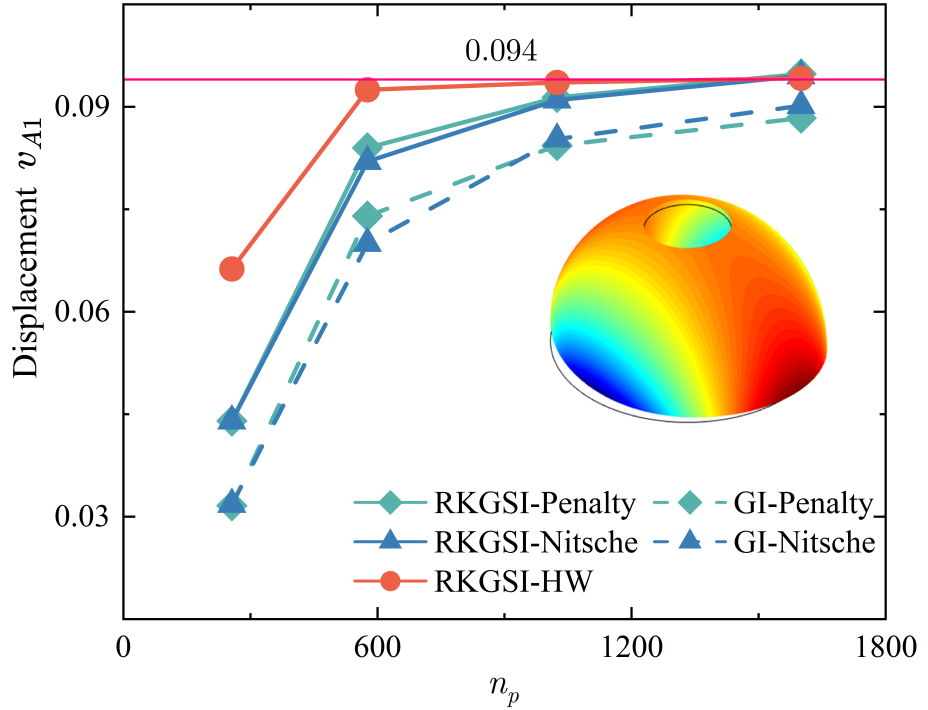


Figure 11: Displacement convergence for pinched hemispherical shell problem.

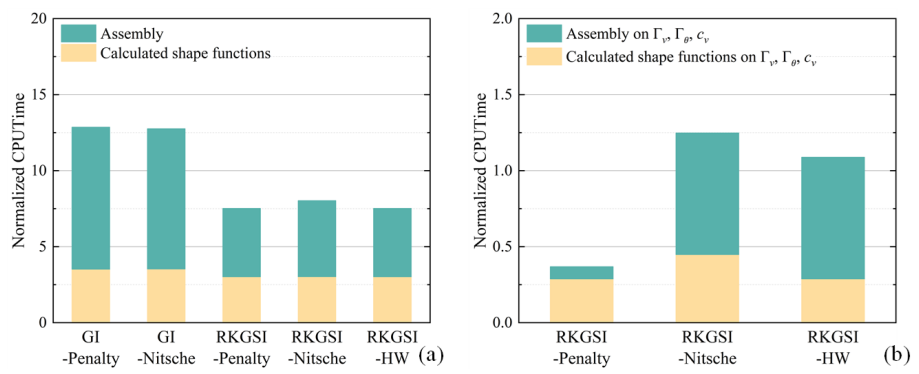


Figure 12: efficiency comparison for pinched hemispherical shell problem: (a) Whole domain; (b) Essential boundaries

415 **6. Conclusion**

416 In this study, an efficient and quasi-consistent meshfree thin shell formu-
417 lation was presented to naturally enforce the essential boundary conditions.
418 Mixed formulation with the Hu-Washizu principle weak form is adopted, where
419 the traditional meshfree shape functions discretized the displacement, and the
420 strains and stresses were expressed by the reproducing kernel smoothed gradi-
421 ents and the covariant smoothed gradients, respectively. The smoothed gradient
422 naturally embedded the first second-order integration constraints and has
423 a quasi variational consistency for the curved models in each integration cell.
424 Owing to the Hu-Washizu variational principle, the essential boundary condi-
425 tion enforcement has a similar form with the conventional Nitsche's method;
426 both have consistent and stabilized terms. The costly high order derivatives in
427 the Nitsche's consistent term have been replaced by the smoothed gradients,
428 which improved the computational speed due to the reproducing kernel gradi-
429 ent smoothing framework. Furthermore, the stabilized term naturally existed
430 in the Hu-Washizu weak form, and the artificial parameter needed in Nitsche's
431 stabilized term has vanished, which can automatically maintain the coercivity
432 for the stiffness matrix. Based on general reproducing kernel gradient smooth-
433 ing framework, the proposed methodology can be trivially extended to high
434 order basis meshfree formulation. The numerical results demonstrated that the
435 proposed Hu-Washizu quasi-consistent meshfree thin shell formulation showed
436 excellent accuracy, efficiency, and stability.

⁴³⁷ **Acknowledgment**

⁴³⁸ The support of this work by the National Natural Science Foundation of
⁴³⁹ China (12102138, 52350410467) and the Natural Science Foundation of Fujian
⁴⁴⁰ Province of China (2023J01108, 2022J05056) is gratefully acknowledged.

⁴⁴¹ **Appendix A. Green's theorems for in-plane vector**

⁴⁴² This Appendix discusses two kinds of Green's theorems used for the development
⁴⁴³ of the proposed meshfree method. For an arbitrary vectors v^α and a
⁴⁴⁴ scalar function f , with Green's theorem for in-plane vector, the first Green's
⁴⁴⁵ theorem is listed as follows [30]:

$$\begin{aligned} \int_{\Omega} f_{,\alpha} v^\alpha d\Omega &= \int_{\Gamma} f v^\alpha n_\alpha d\Gamma - \int_{\Omega} f(v_{,\alpha}^\alpha + \Gamma_{\beta\alpha}^\beta v^\alpha) d\Omega \\ &= \int_{\Gamma} f v^\alpha n_\alpha d\Gamma - \int_{\Omega} f v^\alpha|_\alpha d\Omega \end{aligned} \quad (\text{A.1})$$

⁴⁴⁶ where $\Gamma_{\alpha\beta}^\gamma = \mathbf{a}_{\alpha,\beta} \cdot \mathbf{a}^\gamma$ denotes the Christoffel symbol of the second kind. $v^\alpha|_\alpha$
⁴⁴⁷ can be represented as the in-plane covariant derivative of the vector v^α :

$$v^\alpha|_\alpha = v_{,\alpha}^\alpha + \Gamma_{\beta\alpha}^\beta v^\alpha \quad (\text{A.2})$$

⁴⁴⁸ The second Green's theorem is established with a mixed form of second
⁴⁴⁹ order derivative. Let $A^{\alpha\beta}$ can be an arbitrary symmetric second order tensor,
⁴⁵⁰ the Green's theorem yields [30]:

$$\begin{aligned} \int_{\Omega} f_{,\alpha}|_\beta A^{\alpha\beta} d\Omega &= \int_{\Gamma} f_{,\gamma} n^\gamma A^{\alpha\beta} n_\alpha n_\beta d\Gamma - \int_{\Gamma} f(A^{\alpha\beta} s_\alpha n_\beta)_{,\gamma} s^\gamma d\Gamma + [[f A^{\alpha\beta} s_\alpha n_\beta]]_{\mathbf{x}\in C} \\ &\quad - \int_{\Gamma} f(A_{,\beta}^{\alpha\beta} n_\alpha + \Gamma_{\alpha\beta}^\gamma A^{\alpha\beta} n_\gamma + \Gamma_{\gamma\beta}^\gamma A^{\alpha\beta} n_\alpha) d\Gamma \\ &\quad + \int_{\Omega} f \left(\begin{array}{l} \Gamma_{\alpha\beta,\gamma}^\gamma A^{\alpha\beta} + \Gamma_{\alpha\beta}^\gamma A^{\alpha\beta} + \Gamma_{\eta\gamma}^\eta \Gamma_{\alpha\beta}^\gamma A^{\alpha\beta} \\ + A_{,\alpha\beta}^{\alpha\beta} + \Gamma_{\gamma\beta,\alpha}^\gamma A^{\alpha\beta} + 2\Gamma_{\gamma\alpha}^\gamma A_{,\beta}^{\alpha\beta} + \Gamma_{\gamma\alpha}^\gamma \Gamma_{\eta\beta}^\eta A^{\alpha\beta} \end{array} \right) d\Omega \\ &= \int_{\Gamma} f_{,\gamma} n^\gamma A^{\alpha\beta} n_\alpha n_\beta d\Gamma - \int_{\Gamma} f(A^{\alpha\beta} s_\alpha n_\beta)_{,\gamma} s^\gamma d\Gamma + [[f A^{\alpha\beta} s_\alpha n_\beta]]_{\mathbf{x}\in C} \\ &\quad - \int_{\Gamma} f A^{\alpha\beta}|_\beta n_\alpha d\Gamma + \int_{\Omega} f A^{\alpha\beta}|_\alpha n_\beta d\Omega \end{aligned} \quad (\text{A.3})$$

⁴⁵¹ with

$$A^{\alpha\beta}|_\beta = A_{,\beta}^{\alpha\beta} + \Gamma_{\beta\gamma}^\alpha A^{\beta\gamma} + \Gamma_{\gamma\beta}^\alpha A^{\alpha\beta} \quad (\text{A.4})$$

$$\begin{aligned} A^{\alpha\beta}|_{\alpha\beta} &= \Gamma_{\alpha\beta,\gamma}^\gamma A^{\alpha\beta} + \Gamma_{\alpha\beta}^\gamma A^{\alpha\beta} + \Gamma_{\eta\gamma}^\eta \Gamma_{\alpha\beta}^\gamma A^{\alpha\beta} \\ &\quad + A_{,\alpha\beta}^{\alpha\beta} + \Gamma_{\gamma\beta,\alpha}^\gamma A^{\alpha\beta} + 2\Gamma_{\gamma\alpha}^\gamma A_{,\beta}^{\alpha\beta} + \Gamma_{\gamma\alpha}^\gamma \Gamma_{\eta\beta}^\eta A^{\alpha\beta} \end{aligned} \quad (\text{A.5})$$

⁴⁵³ For the sake of brevity, the notion of covariant derivative is extended to a
⁴⁵⁴ scalar function as:

$$f|_\alpha = f_{,\alpha} + \Gamma_{\beta\alpha}^\beta f \quad (\text{A.6})$$

$$f|_\beta n_\alpha = f_{,\beta} n_\alpha + \Gamma_{\alpha\beta}^\gamma f n_\gamma + \Gamma_{\gamma\beta}^\gamma f n_\alpha \quad (\text{A.7})$$

$$\begin{aligned} f|_{\alpha\beta} &= \Gamma_{\alpha\beta,\gamma}^\gamma f + \Gamma_{\alpha\beta}^\gamma f_{,\gamma} + \Gamma_{\eta\gamma}^\eta \Gamma_{\alpha\beta}^\gamma f \\ &\quad + f_{,\alpha\beta} + \Gamma_{\gamma\beta,\alpha}^\gamma f + 2\Gamma_{\gamma\alpha}^\gamma f_{,\beta} + \Gamma_{\gamma\alpha}^\gamma \Gamma_{\eta\beta}^\eta f \end{aligned} \quad (\text{A.8})$$

⁴⁵⁷ **Appendix B. Derivations for stiffness metrics and force vectors**

⁴⁵⁸ This Appendix details the derivations of stiffness matrices and force vectors
⁴⁵⁹ in Eqs. (53)-(55), where the relationships of Eqs. (40), (41), (44) and (46) are
⁴⁶⁰ used herein. Firstly, the membrane strain terms are considered as follows:

$$\begin{aligned}
 & \sum_{C=1}^{n_e} \int_{\Omega_C} \delta \tilde{\varepsilon}_{\alpha\beta}^h h C^{\alpha\beta\gamma\eta} \tilde{\varepsilon}_{\gamma\eta}^h d\Omega \\
 &= \sum_{C=1}^{n_e} \sum_{I,J=1}^{n_p} \delta \mathbf{d}_I \cdot \underbrace{\int_{\Omega_C} \tilde{\varepsilon}_{\alpha\beta I} h C^{\alpha\beta\gamma\eta} \mathbf{a}_\gamma \mathbf{q}^T d\Omega \mathbf{G}^{-1} \bar{\mathbf{g}}_{\eta J} \cdot \mathbf{d}_J}_{\tilde{\mathbf{g}}_I^{\eta T}} \\
 &= \sum_{C=1}^{n_e} \sum_{I,J=1}^{n_p} \delta \mathbf{d}_I \cdot \underbrace{\int_{\Gamma_C \cap \Gamma_v} \Psi_J \mathbf{q}^T \mathbf{G}^{-1} \tilde{\mathbf{g}}_I^\alpha n_\alpha d\Gamma}_{\tilde{\mathbf{T}}_{NI}} \cdot \mathbf{d}_J \\
 &= \sum_{I,J=1}^{n_p} \delta \mathbf{d}_I \cdot \int_{\Gamma_v} \tilde{\mathbf{T}}_{NI} \Psi_J d\Gamma \cdot \mathbf{d}_J
 \end{aligned} \tag{B.1}$$

⁴⁶¹ with

$$\tilde{\mathbf{g}}_I^\alpha = \mathbf{q} \mathbf{a}_\beta h C^{\alpha\beta\gamma\eta} \tilde{\varepsilon}_{\gamma\eta I} \tag{B.2}$$

$$\tilde{\mathbf{T}}_{NI} = \mathbf{q}^T \mathbf{G}^{-1} \tilde{\mathbf{g}}_I^\alpha n_\alpha \tag{B.3}$$

⁴⁶³ Following this path, the bending strain terms can be reorganized by:

$$\begin{aligned}
 & \sum_{C=1}^{n_e} \int_{\Omega_C} \delta \tilde{\kappa}_{\alpha\beta}^h \frac{h^3}{12} C^{\alpha\beta\gamma\eta} \tilde{\kappa}_{\gamma\eta}^h d\Omega \\
 &= \sum_{C=1}^{n_e} \sum_{I,J=1}^{n_p} \delta \mathbf{d}_I \cdot \underbrace{\int_{\Omega_C} \tilde{\kappa}_{\alpha\beta I} \frac{h^3}{12} C^{\alpha\beta\gamma\eta} \mathbf{a}_3 \mathbf{q}^T d\Omega \mathbf{G}^{-1} \bar{\mathbf{g}}_{\gamma\eta J} \cdot \mathbf{d}_J}_{\tilde{\mathbf{g}}_I^{\gamma\eta T}} \\
 &= \sum_{C=1}^{n_e} \sum_{I,J=1}^{n_p} \delta \mathbf{d}_I \cdot \left(\begin{array}{l} \int_{\Gamma_C \cap \Gamma_\theta} \underbrace{\mathbf{q}^T \mathbf{G}^{-1} \tilde{\mathbf{g}}_I^{\alpha\beta} n_\alpha n_\beta}_{\tilde{\mathbf{M}}_{nnI}} n^\gamma \Psi_{J,\gamma} d\Gamma \\ - \int_{\Gamma_C \cap \Gamma_v} \underbrace{(\mathbf{q}_{\beta}^T \mathbf{G}^{-1} \tilde{\mathbf{g}}_I^{\alpha\beta} n_\alpha + (\mathbf{q}^T \mathbf{G}^{-1} \tilde{\mathbf{g}}_I^{\alpha\beta} s_\alpha n_\beta)_{,\gamma} s^\gamma)}_{\tilde{\mathbf{T}}_{MI}} \Psi_J d\Gamma \\ + [[\underbrace{\mathbf{q}^T \mathbf{G}^{-1} \tilde{\mathbf{g}}_I^{\alpha\beta} s_\alpha n_\beta}_{\tilde{\mathbf{P}}_I \mathbf{a}_3} \Psi_J]]_{\mathbf{x} \in C_C \cap C_v} \end{array} \right) \cdot \mathbf{d}_J \\
 &= \sum_{I,J=1}^{n_p} \delta \mathbf{d}_I \cdot \left(\int_{\Gamma_\theta} \tilde{\mathbf{M}}_{nnI} n^\gamma \Psi_{J,\gamma} d\Gamma - \int_{\Gamma_v} \tilde{\mathbf{T}}_{MI} \Psi_J d\Gamma + [[\tilde{\mathbf{P}}_I \Psi_J]]_{\mathbf{x} \in C_v} \right)
 \end{aligned} \tag{B.4}$$

⁴⁶⁴ with

$$\tilde{\mathbf{g}}_I^{\alpha\beta} = \int_{\Omega_C} \mathbf{q} \frac{h^3}{12} C^{\alpha\beta\gamma\eta} \mathbf{a}_3 \tilde{\boldsymbol{\kappa}}_{\gamma\eta I} d\Omega \quad (\text{B.5})$$

⁴⁶⁵

$$\begin{cases} \tilde{M}_{nnI} = \mathbf{q}^T \mathbf{G}^{-1} \tilde{\mathbf{g}}_I^{\alpha\beta} n_\alpha n_\beta \\ \tilde{T}_{MI} = \mathbf{q}_{|\beta}^T \mathbf{G}^{-1} \tilde{\mathbf{g}}_I^{\alpha\beta} n_\alpha + (\mathbf{q}^T \mathbf{G}^{-1} \tilde{\mathbf{g}}_I^{\alpha\beta} s_\alpha n_\beta)_{,\gamma} s^\gamma \\ \tilde{P}_I = \mathbf{q}^T \mathbf{G}^{-1} \tilde{\mathbf{g}}_I^{\alpha\beta} s_\alpha n_\beta \cdot \mathbf{a}_3 \end{cases} \quad (\text{B.6})$$

466 **References**

- 467 [1] L. H. Donnell, Beams, Plates and Shells, McGraw-Hill, 1976.
- 468 [2] T. J. Hughes, The Finite Element Method: Linear Static and Dynamic
469 Finite Element Analysis, Dover Publications, Mineola, New York, 2000.
- 470 [3] T. Belytschko, Y. Y. Lu, L. Gu, Element-free Galerkin methods, International
471 Journal for Numerical Methods in Engineering 37 (1994) 229–256.
- 472 [4] W. K. Liu, S. Jun, Y. F. Zhang, Reproducing kernel particle methods,
473 International Journal for Numerical Methods in Fluids 20 (1995) 1081–
474 1106.
- 475 [5] J. S. Chen, M. Hillman, S. W. Chi, Meshfree methods: Progress made after
476 20 Years, Journal of Engineering Mechanics 143 (2017) 04017001.
- 477 [6] P. Krysl, T. Belytschko, Analysis of thin shells by the Element-Free
478 Galerkin method, International Journal of Solids and Structures 33 (1996)
479 3057–3080.
- 480 [7] G. R. Liu, Meshfree Methods: Moving Beyond the Finite Element Method,
481 Second Edition, Crc Press, 2009.
- 482 [8] X. Zhang, K. Z. Song, M. W. Lu, X. Liu, Meshless methods based on
483 collocation with radial basis functions, Computational Mechanics 26 (2000)
484 333–343.
- 485 [9] D. Millán, A. Rosolen, M. Arroyo, Thin shell analysis from scattered points
486 with maximum-entropy approximants, International Journal for Numerical
487 Methods in Engineering 85 (2011) 723–751.
- 488 [10] L. Wang, M. Hu, Z. Zhong, F. Yang, Stabilized Lagrange Interpolation
489 Collocation Method: A meshfree method incorporating the advantages of
490 finite element method, Computer Methods in Applied Mechanics and En-
491 gineering 404 (2023) 115780.
- 492 [11] P. Suchde, T. Jacquemin, O. Davydov, Point Cloud Generation for Mesh-
493 free Methods: An Overview, Archives of Computational Methods in Engi-
494 neering 30 (2022) 889–915.
- 495 [12] L. Deng, D. Wang, An accuracy analysis framework for meshfree collocation
496 methods with particular emphasis on boundary effects, Computer Methods
497 in Applied Mechanics and Engineering 404 (2023) 115782.
- 498 [13] J. Wang, M. Hillman, Upwind reproducing kernel collocation method for
499 convection-dominated problems, Computer Methods in Applied Mechanics
500 and Engineering 420 (2024) 116711.

- 501 [14] S. Fernández-Méndez, A. Huerta, Imposing essential boundary conditions
 502 in mesh-free methods, Computer Methods in Applied Mechanics and En-
 503 gineering 193 (2004) 1257–1275.
- 504 [15] X. Li, Error estimates for the moving least-square approximation and the
 505 element-free Galerkin method in n-dimensional spaces, Applied Numerical
 506 Mathematics 99 (2016) 77–97.
- 507 [16] J. Wu, D. Wang, An accuracy analysis of Galerkin meshfree methods ac-
 508 counting for numerical integration, Computer Methods in Applied Mechan-
 509 ics and Engineering 375 (2021) 113631.
- 510 [17] J. S. Chen, H. P. Wang, New boundary condition treatments in meshfree
 511 computation of contact problems, Computer Methods in Applied Mechan-
 512 ics and Engineering 187 (2000) 441–468.
- 513 [18] D. Liu, Y. M. Cheng, The interpolating element-free Galerkin (IEFG)
 514 method for three-dimensional potential problems, Engineering Analysis
 515 with Boundary Elements 108 (2019) 115–123.
- 516 [19] V. Ivannikov, C. Tiago, P. M. Pimenta, On the boundary conditions of the
 517 geometrically nonlinear Kirchhoff–Love shell theory, International Journal
 518 of Solids and Structures 51 (2014) 3101–3112.
- 519 [20] Y. Y. Lu, T. Belytschko, L. Gu, A new implementation of the element free
 520 Galerkin method, Computer Methods in Applied Mechanics and Engineer-
 521 ing 113 (1994) 397–414.
- 522 [21] T. Zhu, S. N. Atluri, A modified collocation method and a penalty formu-
 523 lation for enforcing the essential boundary conditions in the element free
 524 Galerkin method, Computational Mechanics 21 (1998) 211–222.
- 525 [22] S. Skatulla, C. Sansour, Essential boundary conditions in meshfree methods
 526 via a modified variational principle: Applications to shell computations,
 527 Computer Assisted Mechanics and Engineering Sciences 15 (2008) 123–142.
- 528 [23] J. S. Chen, C. T. Wu, S. Yoon, Y. You, A stabilized conforming nodal
 529 integration for Galerkin mesh-free methods, International Journal for Nu-
 530 matical Methods in Engineering 50 (2001) 435–466.
- 531 [24] J. S. Chen, M. Hillman, M. Rüter, An arbitrary order variationally consis-
 532 tent integration for Galerkin meshfree methods, International Journal for
 533 Numerical Methods in Engineering 95 (2013) 387–418.
- 534 [25] Q. Duan, X. Li, H. Zhang, T. Belytschko, Second-order accurate derivatives
 535 and integration schemes for meshfree methods, International Journal for
 536 Numerical Methods in Engineering 92 (2012) 399–424.

- 537 [26] D. Wang, J. Wu, An inherently consistent reproducing kernel gradient
538 smoothing framework toward efficient Galerkin meshfree formulation with
539 explicit quadrature, Computer Methods in Applied Mechanics and Engi-
540 neering 349 (2019) 628–672.
- 541 [27] J. Wang, X. Ren, A consistent projection integration for Galerkin meshfree
542 methods, Computer Methods in Applied Mechanics and Engineering 414
543 (2023) 116143.
- 544 [28] J. Wu, X. Wu, Y. Zhao, D. Wang, A consistent and efficient method for
545 imposing meshfree essential boundary conditions via hellinger-reissner vari-
546 ational principle., Chinese Journal of Theoretical and Applied Mechanics
547 54 (2022) 3283–3296.
- 548 [29] J. Wu, X. Wu, Y. Zhao, D. Wang, A rotation-free Hellinger-Reissner mesh-
549 free thin plate formulation naturally accommodating essential boundary
550 conditions, Engineering Analysis with Boundary Elements 154 (2023) 122–
551 140.
- 552 [30] J. Benzaken, J. A. Evans, S. F. McCormick, R. Tamstorf, Nitsche’s method
553 for linear Kirchhoff–Love shells: Formulation, error analysis, and verifica-
554 tion, Computer Methods in Applied Mechanics and Engineering 374 (2021)
555 113544.
- 556 [31] H. Dah-wei, A method for establishing generalized variational principle,
557 Applied Mathematics and Mechanics 6 (1985) 501–509.
- 558 [32] H. Du, J. Wu, D. Wang, J. Chen, A unified reproducing kernel gradient
559 smoothing Galerkin meshfree approach to strain gradient elasticity, Com-
560 putational Mechanics 70 (2022) 73–100.
- 561 [33] J. Kiendl, K. U. Bletzinger, J. Linhard, R. Wüchner, Isogeometric shell
562 analysis with Kirchhoff–Love elements, Computer Methods in Applied Me-
563 chanics and Engineering 198 (2009) 3902–3914.